Faculté des Bioingénieurs

Expression of genes involved in mitochondrial import, homeostasis and apoptosis.

Présenté par Pauline De Jaeger

Promoteur(s): Prof. Melissa Page (UCL/IBST)
Prof. Jean-François Rees (UCL/IBST)

Lecteurs : Prof. Isabelle Donnay (UCL/IBST)
Prof. Bernard Knoops (UCL/IBST)

Mémoire de fin d'études présenté en vue de l'obtention du diplôme de **Bioingénieur : sciences agronomiques.**

Année académique 2017-2018

Acknowledgments

First of all, I would like to thank my supervisor, Mrs Melissa Page for her precious advice, the transmission of her knowledge and her encouragement. I've learned a lot of new technics, improved my English and it allowed me to realize this interesting master thesis in the BNTE laboratory.

A big thank to my co-supervisor, Mr Jean-François Rees who accepted, despite my very late request, to fulfill this role. His encouragement and advice helped me a lot to improve my work.

I am grateful to Professors Isabelle Donnay and Bernard Knoops for accepting to be members of my jury.

A special thank you goes to the killifish team at KU Leuven for the time they invested in feeding the fish, their help and for giving me access to their laboratory to dissect the fish I needed.

I want to thank greatly Mrs Marine Delsaute and Mrs Vasiliki Argyropoulou, PhD students from Bernard Knoops' lab, for helping me with the agarose gel.

I also want to thank all the members and students of the BNTE for their kindness and their warm welcome.

Finally, I would like to thank my family and my entourage for their big encouragement and their support all along this year.

Table of content

List of abbreviations

AD	Alzheimer's disease
APP	Amyloid precursor protein
Bak	Bcl-2 homologous antagonist killer protein
Bax	Bcl-2-associated X protein
Caspases	Cysteine aspartic proteases
CAT	Catalase
CtTA	C-terminal tail anchor sequence
GPx	Glutathione peroxidase
HSP	Heat shock protein
IMS	Intermembrane space
MnSOD	Manganese SOD
MOMP	Mitochondrial outer membrane permeabilization
MPTP	Mitochondrial permeability transition pore
mtDNA	Mitochondrial DNA
mthsp	Mitochondrial heat shock proteins
OMM	Outer mitochondrial membrane
OXPHOS	Oxidative phosphorylation
PD	Parkinson's disease
ROS	Reactive oxygen species
SD	Standard deviation
SM	Skeletal muscle
SOD	Superoxide dismutase
T2D	Type 2 diabetes
TIM	Translocase of the inner mitochondrial membrane
TNFα	Tumour necrosis factor alpha
TOM	Translocase of the outer mitochondrial membrane

List of figures

List of tables

1. Introduction

Today people are living longer than they have ever before, primarily due to technical and scientific progress, which has resulted in improved hygiene and medical advances. According to the United Nations, the global ageing population, which is defined as those of 60 years of age and older, accounted for approximately 62 million individuals in 2017. By 2050, nearly 17% of the global population is believed to fall within the 65-and-over age bracket, equating to a doubling of aged individuals compared to 2018 (Davies, 2016) and it is predicted, that by 2100, 3.1 billion individuals will be over 60 years of age (Figure 1) (United Nations).

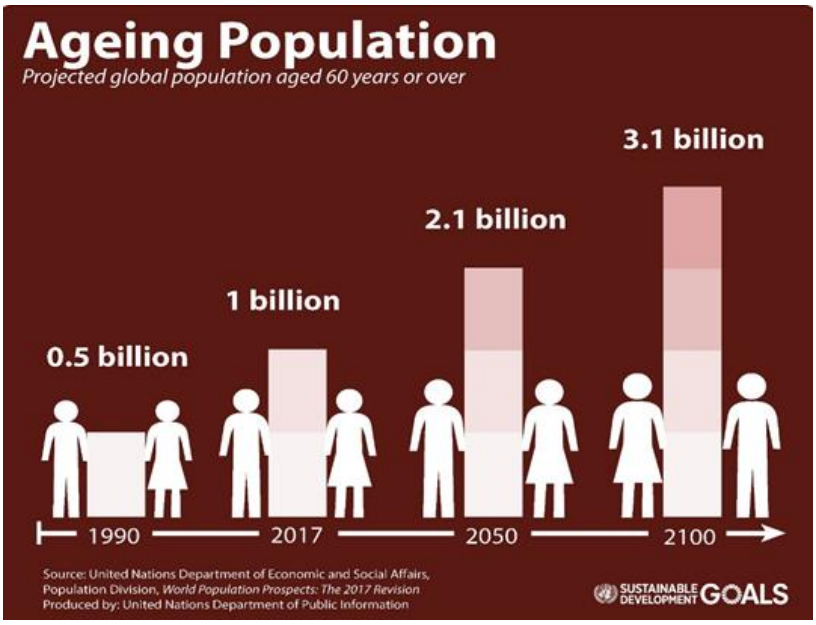

Figure 1: **The projected global population of individuals aged 60 years of age and over.** (United Nations, 2017)

Longer lives however are often not matched with a high quality of life in later years, as older individuals are more susceptible to chronic and debilitating diseases, such as cancer, neurodegenerative disease and metabolic disorders. It is important that we understand the underlying factors associated with ageing and how ageing impacts these diseases to find novel treatments to improve health throughout the life of an individual.

Ageing is the fundamental biological process of becoming older (Kim *et al*, 2016). It has been defined as the time-dependent decline of functional capacity and stress resistance, associated with an increased risk for different diseases (Bürkle *et al*, 2015; Kim *et al*, 2016). The ageing process is due to internal physiological deterioration and affects all the tissues and organs of the body during the lifespan of the organism (Bürkle *et al*, 2015; Kim *et al*, 2016;

Rose *et al*, 2012), however it remains unclear what are the molecular mechanisms that underlie the physiological deterioration. The rate of ageing varies between individuals of a same species (Bürkle *et al*, 2015) and in the case of humans, can be associated with visible changes such as developing wrinkles and grey hair.

2. State of the art

2.1 Mitochondrial function and its decline with ageing

Mitochondria are important organelles that have been implicated as having a major role in ageing. They have a complex and dynamic internal structure made of six compartments; the outer membrane, the inner boundary membrane, the intermembrane space (IMS), the cristal membrane, the cristae, and the matrix (Logan, 2007) (Figure 2). The cristal membrane is part of the inner membrane system and forms tubules or lamellae in the interior and it is the principal site of oxidative phosphorylation (OXPHOS) (Gilkerson *et al*, 2003). Mitochondria are central to the control of metabolism, regulation and energetic pathways in eukaryotic cells (Wiedemann & Pfanner, 2017). Thus, they play a key role in the production of cellular energy in the form of ATP as well as in crucial cellular processes such as amino acid catabolism, the urea cycle, ketogenesis, calcium cycling and apoptosis (Wiedemann & Pfanner, 2017; Gómez-Serrano *et al*, 2016). The regulation of mitochondrial calcium homeostasis plays an important part in many of the processes involving this organelle (Giorgi *et al*, 2012). For example, isocitrate dehydrogenase and 2-oxoglutarate dehydrogenase, two rate-limiting enzymes of the Krebs cycle, are activated by calcium (Vandecasteele, Szabadkai and Rizzuto, 2001). The Krebs cycle, which occurs in the mitochondrial matrix is a central mechanism required for ATP production and cellular respiration (Smith, 2012). The Krebs cycle is a series of reactions that precede oxidative phosphorylation (OXPHOS) (Smith, 2012). Disruption to calcium homeostasis can therefore affect normal OXPHOS thereby promoting ROS generation and negatively impact cellular physiology (Giorgi *et al*, 2012). This stress affects replication and

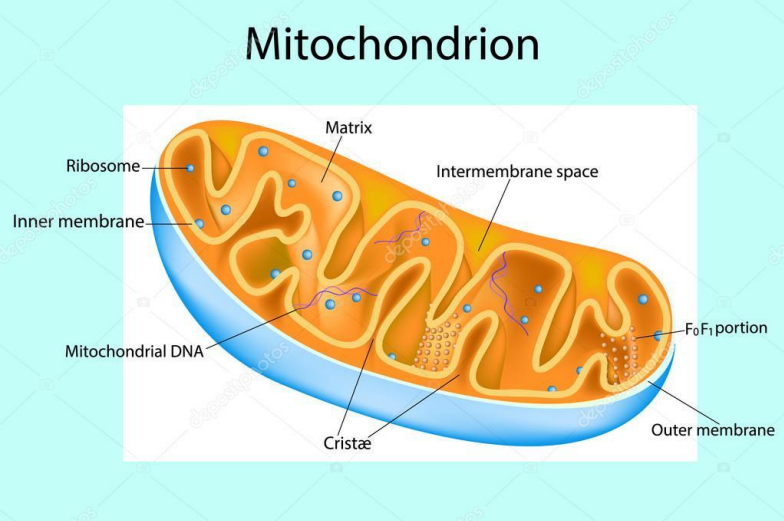

Figure 2: **The different structures and compartments of a typical mitochondrion.** (Sakurra, 2016)

transcription of mitochondrial DNA (mtDNA) and generates mutations to macromolecules (reviewed in Cui *et al*, 2012). Consequently, it results in a decline of mitochondrial function and because of the important role of mitochondria in apoptosis, the accumulation of these damages may influence ageing (reviewed in Cui *et al*, 2012). Ageing is characterized by a progressive loss of organ function, which is highly associated with degenerative disorders, supported by a progressive emergence of apoptosis (Giorgi *et al*, 2012). Throughout the lifespan of most vertebrates, there is a progressive accumulation of molecular damage due to the age-dependent decrease in the force of selection that fails to remove deleterious mutations. This induces a decrease of DNA or protein stability, disruption in energy production and utilization and a loss of homeostasis in the cell, which leads to structural and functional decay (Kim *et al*, 2016). Therefore, impairments to the overall process of ATP generation have been associated with ageing (Giorgi *et al*, 2012). For optimal function, mitochondria rely on proteins encoded from their own genome as well as from the nuclear genome (Figure 3). In vertebrates, the mitochondrial genome encodes only 13 proteins (Lindsay *et al*, 2011), which are all incorporated into the complexes that comprise the electron transport chain and function in OXPHOS to generate ATP. However, approximately 99% of the mitochondrial proteome is made up of nuclear-encoded proteins that must be successfully imported into mitochondria (Wiedemann & Pfanner, 2017). These proteins, function in ATP generation as well as various other roles, such as those involved in oxidative stress protection and apoptosis (Dudek *et al*, 2013). Mitochondria produce reactive oxygen species (ROS) as normal by-products of OXPHOS (University of Helsinki, 2017). Complex I and III (Figure 4A) are the primary production sites of mitochondrial ROS in the form of superoxide radicals (Bratic & Larsson, 2013). Superoxide radicals can further be converted to other compounds including the hydroxyl radical (Figure 4B), which is considered to be the most damaging form of ROS (Bratic & Larsson, 2013). In balanced situations, ROS are

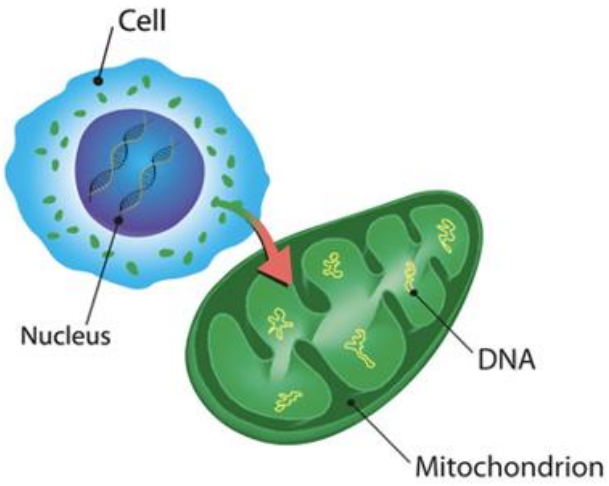

Figure 3: **Mitochondrial proteins are encoded from the nuclear genome and the mitochondrial genome.**

produced during mitochondrial oxidative metabolism as well as a result of environmental factors, such as exposure to toxins and are counterbalanced by antioxidants (Ray *et al*, 2012). Oxidative stress refers to an excess of ROS compared to the capability of the cell to build an effective antioxidant response (Ray *et al*, 2012). Oxidative stress results in the indirect damage of nucleic acids, lipids, and proteins; elevated ROS levels have been implicated in carcinogenesis, neurodegeneration, atherosclerosis, diabetes, and ageing (Ray *et al*, 2012). As mentioned above nuclear-encoded proteins targeted to mitochondria can neutralize ROS (Limón-Pacheco & Gonsebatt, 2009) for example glutathione peroxidase (GPx) and superoxide dismutase (SOD) have both cytosolic and mitochondrial isoforms (Limón-Pacheco & Gonsebatt, 2009). In the latter case, manganese SOD (MnSOD) is localized to the mitochondrial matrix and is believed to act as a first line of defense against oxidative stress from cellular respiration. Other antioxidant enzymes can be found in the matrix as well as in the IMS (Birben *et al*, 2012).

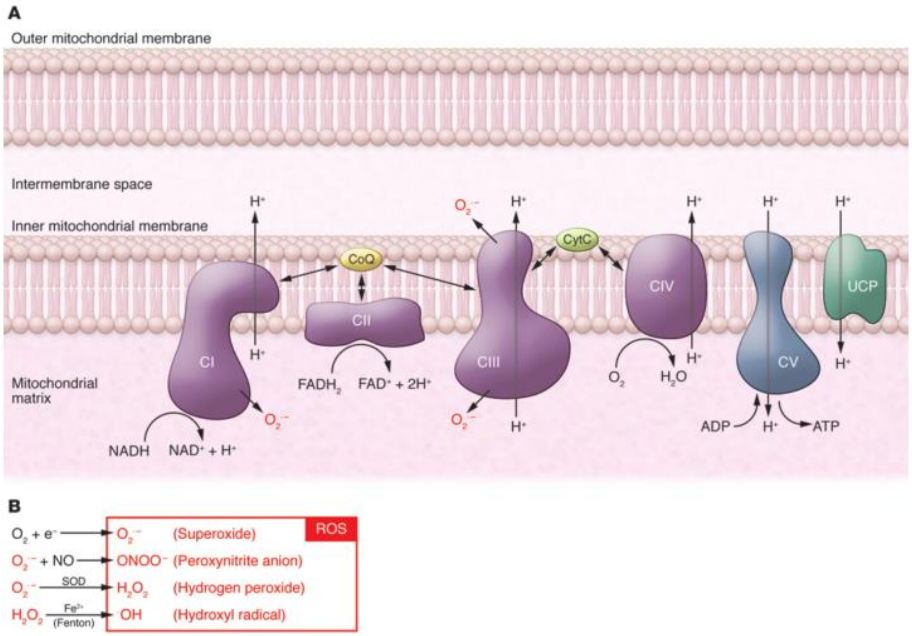

Figure 4: **Schematic model of the oxidative phosphorylation system and the production of ROS.** A) ROS as superoxide radicals can be generated towards the matrix side from both complex I and III as well as towards the IMS from complex III (Bratic & Larsson, 2013). B) Reactions of ROS, note that ROS can be formed following neutralization with an antioxidant enzyme (SOD).

The reason why we age is still not fully understood but dysfunctional mitochondria can lead to reduced ATP levels, a decrease in mtDNA, a decrease of mitochondrial biogenesis and impaired calcium signaling. Taken together, these may lead to oxidative stress and trigger apoptosis, indicating the importance of mitochondrial homeostasis to cell survival. Impaired respiratory chain function and increased ROS levels may contribute to the process of ageing as noted in mice that accumulate mtDNA mutations (Trifunovic & Larsson, 2008a). These mutant mice, which express a homozygous knock-in mutation of the mitochondrial DNA repair

polymerase (PolγA) display early onset of various ageing phenotypes, such as hair loss, curvature of the spine, and weight loss (Trifunovic & Larsson, 2008b). In addition, old heterozygous mice ($MnSOD^{+/-}$) have elevated levels of ROS production accompanied with reduced mitochondrial function, compared with age-matched wild type mice with two copies of MnSOD ($MnSOD^{+/+}$) (Brown *et al.*, 2007). Reduction of MnSOD can lead to an increase of vascular dysfunction in old MnSOD heterozygous mice compared to control mice, which correlates with increased superoxide radical production attributable to mitochondrial dysfunction combined with a decrease in antioxidant capacity (Brown *et al.*, 2007). This suggests that MnSOD heterozygous mice are more prone to ageing phenotypes (Brown *et al*, 2007).

2.2 Mitochondrial import of nuclear-encoded proteins

The majority of nuclear-encoded proteins are synthesized in the cytosol with targeting signals that direct the proteins to mitochondria and into the correct mitochondrial compartment (Wiedemann & Pfanner, 2017). About 60% of these proteins possess a cleavable targeting pre-sequence; the second largest group of nuclear-encoded proteins targeted to mitochondria are characterized by an internal targeting signal, however a pool of proteins remain that are imported into the mitochondria that have no discernible target sequence (Wiedemann & Pfanner, 2017). Mitochondrial destined nuclear-encoded proteins are imported via five separate pathways, the individual pathway is

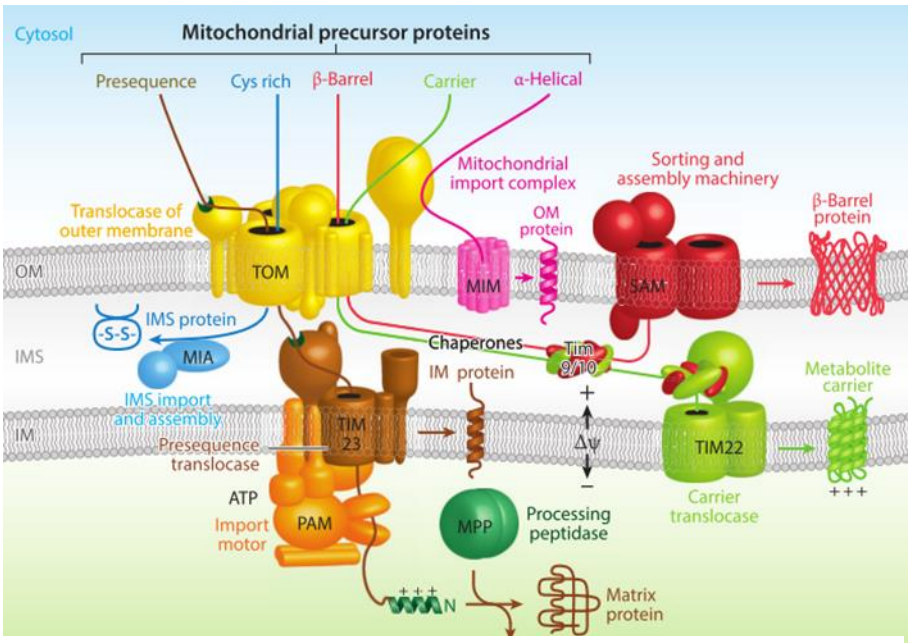

Figure 5: **The five major protein import pathways of mitochondria.** The majority of nuclear-encoded mitochondrial imported proteins enter mitochondria via the pre-sequence pathway, however four alternative pathways occur and depend on the composition and conformation of the imported proteins. The TOM protein complex remains the primary port of entry for the majority of the imported proteins as can be noted in the figure. (Wiedemann, N. *et al.,* 2017)

determined by the presence or absence of a pre-sequence in addition to other factors such as conformation of the targeted protein (Figure 5) (Wiedemann & Pfanner, 2017). Cleavable pre-sequences, which can occur in either the N-terminal or C-terminal of the protein (Diekert *et al*, 1999) are variable in length. Once imported into mitochondria the pre-sequences are cleaved by mitochondrial processing peptidase (MPP) to form mature proteins (Figure 5) (Wiedemann & Pfanner, 2017). The major and classical import pathway relies on the translocase of the outer mitochondrial membrane (TOM) and the translocase of the inner mitochondrial membrane (TIM) (Wiedemann & Pfanner, 2017). In this case, the majority of proteins are synthetized with N-terminal pre-sequences and must be unfolded prior to their import. Upon translocation across the mitochondrial membranes, chaperone proteins function to refold them into their final conformation (Wiedemann & Pfanner, 2017).

Proteins that comprise the TOM and TIM complexes are evolutionarily conserved and are present in all eukaryotes suggesting an important biological function (Lithgow & Schneider, 2010). The TOM complex consists of three receptor proteins (Tom20, Tom22 and Tom70), the channel-forming protein Tom40, and three small Tom proteins (Tom5, Tom6 and Tom7) that maintain structural stability (Figure 6) (Wiedemann & Pfanner, 2017). Tom40 is a β-barrel protein, which forms the transmembrane channel of the complex and interacts with precursor proteins (Wiedemann & Pfanner, 2017). The TIM complex is formed with dynamic multi-subunit machinery that recognizes precursor proteins and that can transport them in two directions, into the inner membrane space or the matrix (Wiedemann & Pfanner, 2017). The core

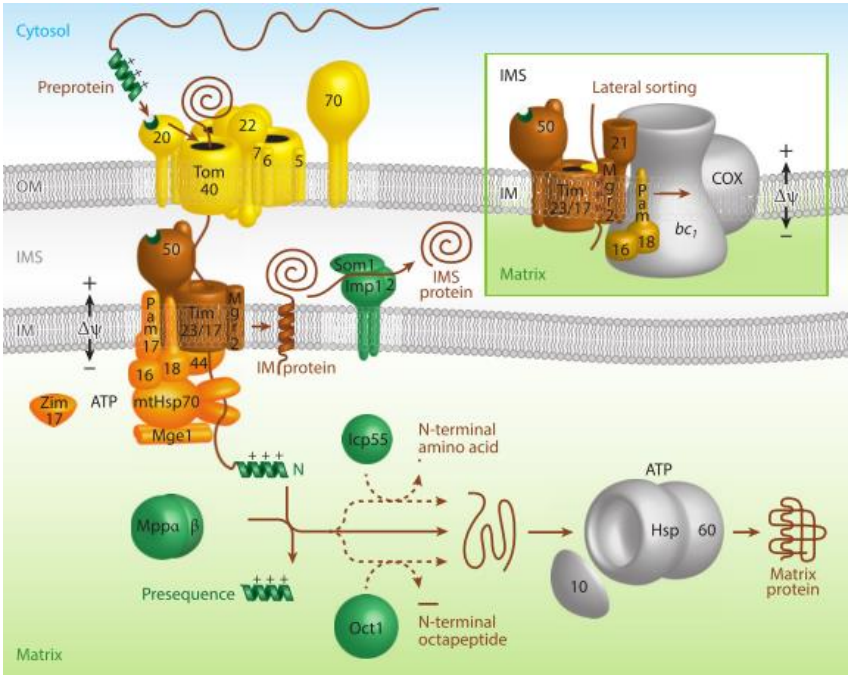

Figure 6: **The pre-sequence pathway into the mitochondrial inner membrane and matrix.** A pre-sequence protein is transported through Tom40, and Tim23 processing can either deliver the protein to the IMS or the matrix. Within the matrix the final conformation of the protein is achieved by chaperone activity, such as from heat shock protein 60 (Hsp60). (Wiedemann, N. *et al., 2017*)

of the TIM complex is comprised of the essential tim23 protein; mice null for tim23 are not viable. Although heterozygous tim23 mice are viable they have reduced survival, indicating a critical role of the import machinery of mitochondria (Ahting *et al*, 2009). Other studies have also demonstrated the important of the TIM23 complex. *C. elegans* mutants with loss-of-function of TIM23 complex have small bodies, reduced brood size and partial embryonic lethality (Curran *et al*, 2004).

Mitochondrial import has been reported to be impaired in age-related neurodegeneration, such as Alzheimer's disease (AD) and Parkinson's disease (PD). AD can be characterized by the accumulation of beta amyloid polypeptides, which are generated from the proteolysis of amyloid precursor protein (APP). Devi *et al.* (2006) noted that mitochondria isolated from AD affected brain regions have higher levels of APP than mitochondria isolated from aged-matched controls. Furthermore, APP formed stable complexes with TOM and TIM, and impeded the import of nuclear-encoded mitochondrial proteins, leading to impaired ATP generation and increased ROS production (Devi *et al*, 2006). Similarly, α-synuclein, which is implicated in the pathogenesis of PD, has been reported to bind with high affinity to the TOM receptor, TOM20. This stable complex was higher in the brains of PD model mice than within control brains, and was accompanied by reduced ATP generation and increased ROS levels (Di Maio *et al*, 2016; Devi *et al*, 2006). Another example of human age-related disease associated with mitochondrial import dysfunction is type 2 diabetes (T2D) (Gómez-Serrano *et al*, 2016). Protein expression of Tom70 and Tom20 within the TOM complex was significantly reduced in adipose tissue isolated from T2D women compared to age-matched controls. Furthermore, protein and activity of specific OXPHOS complexes was also reduced in these same patients, in contrast, SOD2 and mitochondrial thioredoxin protein was up regulated. (Gómez-Serrano *et al*, 2016). It is unclear if the reduction of Tom70 and Tom20 may modulate the import of specific pools of mitochondrial targeted proteins.

The TOM and TIM complexes are the two main protein complexes that import mitochondrial targeted proteins, whereas mitochondrial heat shock proteins (mthsp) play a large part in delivering these imported proteins to the correct compartments and folding them into their final protein structure (Parcellier *et al*, 2003). Studies have shown that these proteins are essential for life and are well-conserved across species (reviewed in Leak, 2014).Mitochondrial hsp60 (mthsp60) is also involved in mitochondrial protein import and assembly (Parcellier *et al*, 2003), stabilizing and folding imported proteins destined for the

matrix (Figure 5) (Wiedemann & Pfanner, 2017). Mitochondrial hsp70 (mthsp70) also plays an important role in protein import as well as folding and assembly of the nuclear-encoded proteins in the mitochondrial matrix (Herrmann *et al*, 1994). It acts as a chaperone for the mitochondrial encoded subunits of the ATP synthase complex, and has a key role in the assembly of supra-molecular complexes, which are bound together by noncovalent bounds (Herrmann *et al*, 1994). Several studies noted that a loss-of-function of mthsp60 or mthsp70 are associated with pathological processes such as cardiovascular or neurodegenerative diseases (Campos *et al*, 2016; Leak, 2014). Heat shock protein 70 has a protective role in many experimental disease models such as Parkinson's where it enhances α-synuclein refolding and/or degradation and therefore decreases α-synuclein toxicity (reviewed in Leak, 2014). The activity and availability of Hsp70 decreases with age in neuronal tissue, possibly suggesting that hsp70 may have a protective effect against ageing. Exogenous and long term intranasal administration of human Hsp70 significantly increased the lifespan of mice when initiated at 17 months of age (Bobkova *et al*, 2015).

2.3 Apoptosis

Proteins involved in apoptosis are among some of those that are imported into mitochondria. Apoptosis is a genetically programmed and regulated type of cell death (Renehan *et al*, 2001). It is a controlled and energy-dependent phenomenon that can affect individual or groups of cells (reviewed in Elmore, 2007). Apoptosis governs several biological processes that range from embryogenesis to ageing, from homeostasis to diseases (Renehan *et al*, 2001; Wang & Youle, 2009). It has also a complementary and opposite role to cell proliferation and mitosis (reviewed in Elmore, 2007). Some cells, such as neurons and cardiac cells have very low levels of proliferation and high levels of apoptosis are considered deleterious in the organs that are comprised of these cells (Warner, 1997). However, apoptosis may also be beneficial as this process can eliminate dysfunctional cells which may have the possibility to be replaced by cell proliferation to maintain homeostasis (Warner, 1997; Smith *et al*, 2017). With increased age, it has been observed that there is a decrease in the potential of apoptosis in tissues with a high turnover such as epithelial cells and this may lead to an increase of cancer incidence (Warner, 1997). In most cells, there is a balance between cell proliferation and apoptosis, it seems that to maintain homeostasis in the adult

human body, approximately 10 billion cells are made each day (reviewed in Elmore, 2007). To maintain homeostasis, cell production can increase to match elevated levels of apoptosis, for example during normal development, ageing and/or during diseases (reviewed in Elmore, 2007). Evidence suggests that the accumulation of oxidative damage in neurons and cardiac cells plays a role in age-induced apoptosis (reviewed in Elmore, 2007). These cells have a really low turnover and are very reliant on ATP production and so, increased ROS production may lead to increased apoptosis and could result in heart attacks and neurodegeneration. Apoptosis can also occur as a mechanism of defense of the cell and the body against invasion by toxins and bacteria (reviewed in Elmore, 2007). The deregulation of this mechanism can lead to cancers, immune diseases or neurodegenerative diseases, such as PD or AD (Renehan, Booth and Potten, 2001; reviewed in Elmore, 2007; Wang and Youle, 2009). Thus, in most cases, it is an essential mechanism to the survival of multicellular organisms.

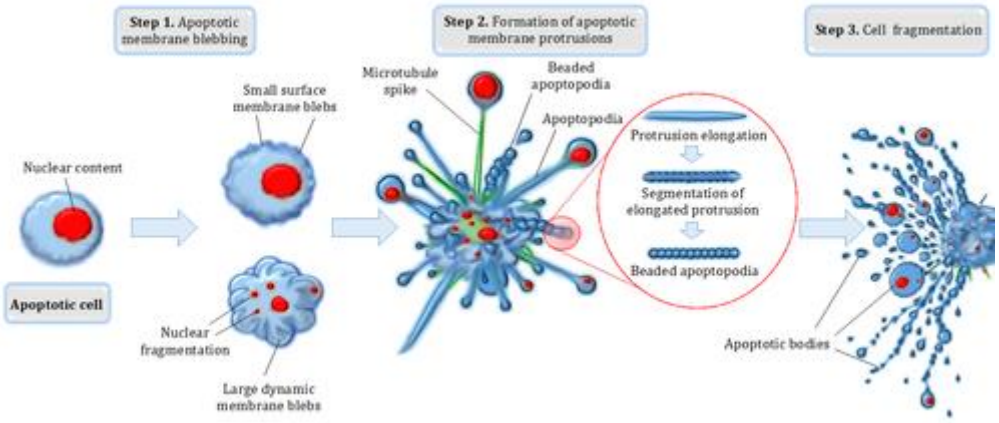

Figure 7: **Different steps in apoptotic cell disassembly.** Step 1) Generation of circular bulges on the cell surface. Step 2) The cell undergoes further morphological changes to generate a variety of thin apoptotic membrane protrusions. Step 3) Release of individual membrane-bound apoptotic bodies, generally considered as approximately 1 to 5 microns in diameter. (Smith *et al*, 2017)

Apoptotic cells are characterized by distinct cell disassembly patterns (Figure 7), including membrane blebbing, cell shrinkage, chromatin condensation and nuclear fragmentation, after which neighbouring cells rapidly engulf the remains of the apoptotic cell (Renehan, Booth and Potten, 2001; Wang and Youle, 2009). At the early stages of apoptosis, cell shrinkage and chromatin condensation are visible by light microscopy: here apoptotic cells are smaller with dense cytoplasm that are more firmly packed (reviewed in Elmore, 2007) compared to non-apoptotic cells. During chromatin condensation, the dense nuclear material usually aggregates peripherally under the nuclear membrane (reviewed in Elmore, 2007).

Following these early stages of apoptosis, cell budding occurs consisting of karyorrhexis, which is the destructive fragmentation of the nucleus (reviewed in Elmore, 2007). Apoptotic bodies are then formed and are comprised of cytoplasm, tightly packed organelles with or without nuclear fragments which are enclosed by an intact plasma membrane (reviewed in Elmore, 2007). Finally, these bodies are phagocytosed by macrophages, parenchymal cells or neoplastic cells and are degraded in phagolysosomes (reviewed in Elmore, 2007).

There are two well-characterized apoptotic pathways (Figure 8); the extrinsic and intrinsic pathways, which converge on the execution pathway, and are initiated by the cleavage of execution caspases (reviewed in Elmore, 2007). Caspase-3 is considered to be the most important of the executioner caspases (reviewed in Elmore, 2007). The extrinsic pathway is triggered by an external signal, for example the binding of tumour necrosis factor alpha (TNFα) to its transmembrane receptor. The binding will induce a signal cascade that leads to an auto-catalytic activation of procaspase-8 which will in turn trigger the cleavage of caspase-3 (cysteine aspartic proteases), leading to the execution phase of apoptosis (reviewed in Elmore, 2007). The intrinsic pathway, in comparison, is initiated by non-receptor-mediated stimuli such as growth factor deprivation, DNA damage or oxidative stress that produce internal signals that proceed directly on cellular targets (reviewed in Elmore, 2007; McIlwain, Berger and Mak, 2013). The stimuli generate intracellular signals that can act either by driving apoptosis (e.g. radiation or toxins) or by failing in the suppression of death programs and thus triggering apoptosis (e.g.

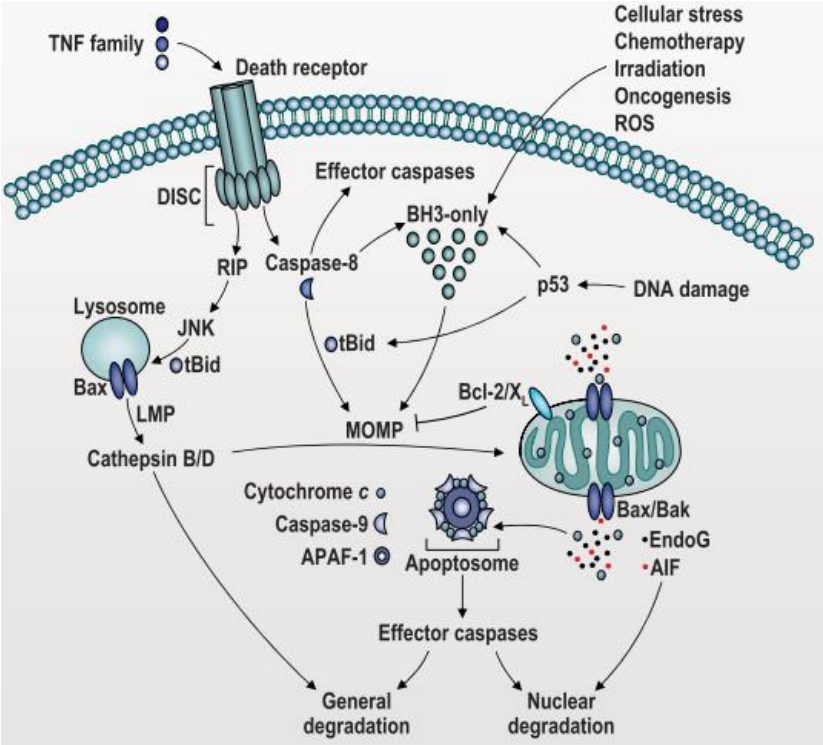

Figure 8: **Extrinsic (initiated via i.e TNFα) and intrinsic (initiated by i.e cellular stress) apoptotic pathways.** The execution pathway commences with the cleavage of the effector caspases (caspase-3 is the most important one). (Vicencio, J. M. *et al.,* 2008)

absence of growth factor, hormones, and/or cytokines) (reviewed in Elmore, 2007). Although the involvement of mitochondria remains central to the initiation of the intrinsic apoptotic pathway, these different stimuli can provoke changes to the inner mitochondrial membrane. This leads to the opening of the mitochondrial permeability transition pore (MPTP), a decrease in the transmembrane potential and a release of pro-apoptotic proteins, such as cytochrome c into the cytosol culminating in the activation of the caspase-dependent pathway (reviewed in Elmore, 2007).

The intrinsic apoptotic pathway is regulated by several proteins of the Bcl-2 family, which contains at least 20 family members (Renehan *et al*, 2001) that are pro-apoptotic (e.g. Bax, Bak) or anti-apoptotic (e.g. Bcl-2, Bcl-w) (Wang & Youle, 2009). Bcl-2-associated X protein (Bax) and Bcl-2 homologous antagonist killer protein (Bak) are the key regulator targets, therefore many intracellular signals converge on them, and determine the fate of the cell (Wang & Youle, 2009). Studies have shown that when Bcl-2 levels were suppressed in human fibroblasts, cell population doubling was reduced by approximately 15% compared to untreated cells (Kumazaki *et al*, 2002). Population doubling was recovered following the addition of the antioxidant (N-acetyl-L-cysteine), suggesting that ROS were the principal cause of death (Kumazaki *et al*, 2002). Mice that lack functional Ku-70, a DNA repair protein, have early signs of ageing and reduced lifespan, which can be partially recovered with the additional deletion of Bax- (Matsuyama *et al*, 2016). These studies suggest that Bax activity has a significant impact on the short lifespan of the Ku-70 knockout mice (Matsuyama *et al*, 2016).

Bak and bax promote mitochondrial outer membrane permeabilization (MOMP) by oligomerizing to form pores in the outer membrane (Lindsay *et al*, 2011). In a healthy cell, Bax can be found in the outer mitochondrial membrane (OMM) and in the cytosol; upon an apoptotic signal, cytosolic Bax translocates to the OMM whereas Bak persistently resides within mitochondria, anchored to the outer membrane, but goes through a series of conformational changes to form homo- and hetero-dimers with Bax (Wang & Youle, 2009; Lindsay *et al*, 2011). Bcl-2 proteins govern the MPTP and the release of cytochrome c and act to influence whether the cell commits to apoptosis or aborts the process before a currently unknown commitment point (reviewed in Elmore, 2007). In healthy cells, Bcl-2 proteins are found in the cytoplasm and on the OMM (Figure 9) (Lindsay *et al*, 2011). Anti-apoptotic proteins, such as Bcl-2 or Bcl-w, are found on the OMM where they act to inhibit apoptosis

through interaction and inhibition of the pro-apoptotic proteins Bax and Bak (Lindsay *et al*, 2011). Some BH3-only proteins (proteins containing Bcl-2 homology domain number 3) (Bim, Puma and Noxa) and other pro-apoptotic Bcl-2 proteins are up-regulated or post-translationally modified following apoptotic signals and will interact with Bax or Bak once they are present at the mitochondria, to promote cytochrome c release and apoptosis (Lindsay *et al*, 2011). The key role of cytochrome c in the mitochondria is to transport electrons between complexes III and IV (Nicholls *et al*, 2013). Anti-apoptotic members prevent apoptosis by sequestering proforms of caspases (apoptosome) or by preventing the release of mitochondrial apoptogenic factors, such as cytochrome c, into the cytoplasm (Tsujimoto, 1998). In contrast, the pro-apoptotic members signal apoptosis by triggering the activation of caspases via heterodimerization of cleaved procaspases or by inducing the release of apoptogenic factors into the cytoplasm (Tsujimoto, 1998). The majority of Bcl-2 proteins, both pro- and anti-apoptotic, contain a functional C-terminal tail anchor sequence (CtTA) that acts as a mitochondrial targeting sequence (Lindsay *et al*, 2011). Although Bax does not have a functional CtTA it is targeted to mitochondria via an N-terminal pre-sequence.

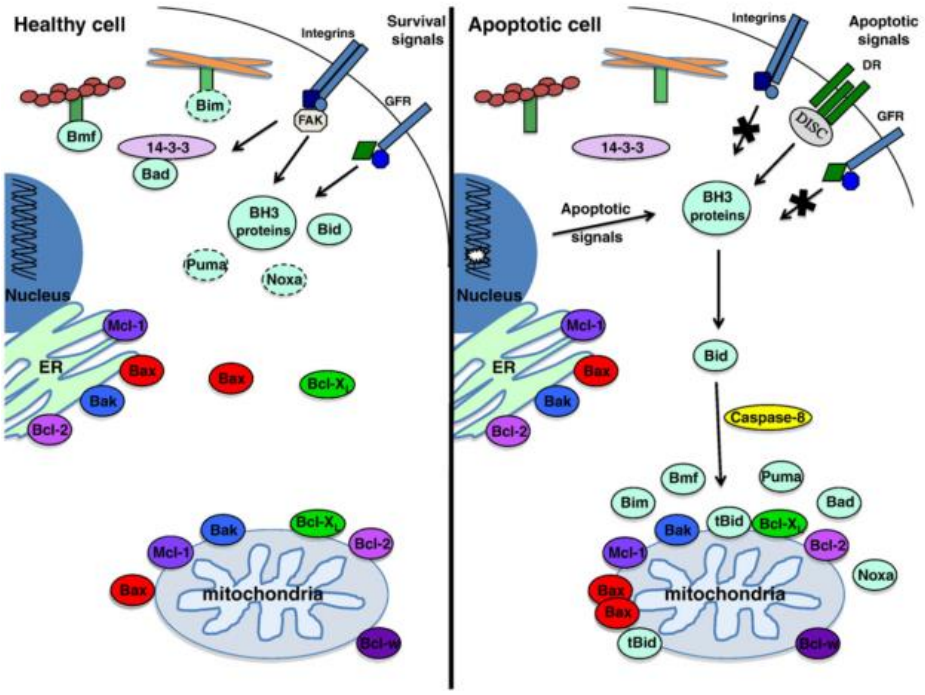

Figure 9: **Localization of Bcl-2 family proteins in a healthy and apoptotic cell.** In an apoptotic cell, Bax and or Bax/Bak will dimerize to form pores in the mitochondrial outer membrane leading to permeabilized mitochondria. The difference between a healthy cell and an apoptotic cell may depend on the ratio of anti- to pro-apoptotic proteins. (Lindsay *et al*, 2011)

Caspases are widely expressed as an inactive monomeric procaspase form in cells (Renehan *et al*, 2001). However, upon dimerization and cleavage of the procaspase enzyme,

they are activated to cleave many cellular substrates (proteins), usually after an aspartate residue in the substrate (Shi, 2004), to dismantle the content of the cells (Renehan *et al*, 2001; Wang & Youle, 2009; McIlwain *et al*, 2013). Caspases have been classified by their important roles in the control of inflammation and cell death (McIlwain *et al*, 2013), but there is currently no evidence to suggest that caspases have overlapping roles in both apoptosis and inflammation. Initiator caspases (8 and 9) cleave and activate executioner caspases (3, 6 and 7) that subsequently coordinate their activities to destroy key structural proteins and activate other enzymes (McIlwain *et al*, 2013).

Mitochondrial function plays a key role in ageing, and dysfunctional mitochondria may induce cellular ageing due to reduced levels of ATP or an imbalance of apoptotic signaling. When dysfunction of mitochondria disturbs cell homeostasis, it leads to a decline in cellular processes and this is a quick definition of ageing. It is currently unknown whether the expression of genes involved in mitochondrial import and apoptosis are correlated with ageing. To address this, animal models may be more appropriate compared to cells in culture because they lose some of their *in vivo* properties for example cell-cell communication can be affected. For example, *C. elegans* and drosophila are widely used invertebrate models to study the progression of cellular ageing. These animals are easy to reproduce and have the advantages of having short lifespans. However certain questions regarding human aging cannot be addressed using these models, for example they are comprised primarily of post-mitotic cells and therefore are not appropriate models to study cancer development. Mice are the most commonly used vertebrate model to study human ageing, however compared to invertebrate models, they have longer lifespans and cost more to maintain. To overcome the above limitations ageing researchers have turned to using the African turquoise killifish, which have quickly become an excellent choice that offers the advantages of a short lifespan while being a vertebrate model.

2.4 The Killifish: a practical model system

African turquoise killifish (*Nothobranchius furzeri*), which will be referred to hereafter as killifish, (Figure 10), are found in seasonal and ephemeral freshwater ponds formed during the short rainy season in semi-arid areas of Mozambique and Zimbabwe (Kim *et al*, 2016;

Valenzano *et al*, 2017; Harel *et al*, 2016). This unique environment has created a selective pressure on the life cycle of killifish and induced a unique set of adaptations, for example, fertilized embryos can survive several months up to years without water, by entering diapause, an arrested state during embryo development (Valenzano *et al*, 2017; Kim *et al*, 2016). In comparison the lifespan of hatched killifish is limited by the rainy season and ranges between 4 to 6 months (Kim *et al*, 2016; Valenzano *et al*, 2017). Killifish reach sexual maturation within 3-4 weeks of birth to assure reproduction before the pending dry season (Valenzano *et al*, 2017; Kim *et al*, 2016). Lifespan studies have reported the impact of environmental conditions, for example killifish strains living in more arid areas have a shorter lifespan whereas strains with habitats in areas with longer rainy seasons have a longer lifespan. Interestingly these lifespans continue to be different in a captive laboratory setting suggesting that it is not just the environment that influences their ageing and lifespan (Valenzano *et al*, 2017). Additionally, the genome differs between killifish strains and this may also influence the lifespan (Valenzano *et al*, 2015). The strains vary between different climates; GRZ strain (Gona Re Zhou National Park in Zimbabwe) and some MZM (from Mozambique) strains are found in a semi-arid area with scarce and erratic precipitation (Terzibasi *et al*, 2008) while some MZM strains are found in areas with more rainfall (Terzibasi *et al*, 2008). The GRZ strain, which is now considered an in-bred strain was originally collected from the field in 1968, we used this strain to address the hypothesis below (Terzibasi *et al*, 2008). The GRZ strain has the shortest recorded lifespan of a vertebrate in captivity with a reported maximum lifespan ranging between 16 and 24 weeks (Terzibasi *et al*, 2008; Kim, Nam and Valenzano, 2016) and is easily reproducible in a lab setting. Furthermore, killifish share several molecular, cellular and physiological ageing phenotypes with humans (Figure 11), such as mitochondrial dysfunction and cancer development (Harel *et al*, 2016). Such as in rodent models of ageing, lifespan can be manipulated by non-genetic interventions such as dietary restriction or through resveratrol supplementation (Harel *et al*, 2016).

Figure 10: **A new model organism for ageing studies.** (Valenzano *et al*, 2017)

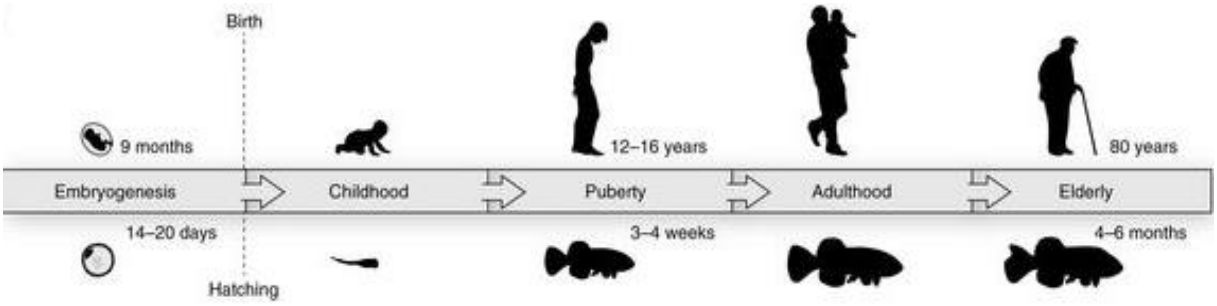

Figure 11: **Timeline that compares the life stages of killifish and humans.** Although embryo development in the killifish can be suspended during diapause the total number of days to complete active embryogenesis ranges between 14-20 days. (Harel et al., 2016)

3. Master thesis aims

In this thesis, we addressed whether the expression of genes involved in mitochondrial import and homeostasis correlate with lifespan by using the African turquoise killifish as an ageing model. To achieve this aim, we have two hypotheses:

- The expression of genes involved in mitochondrial import machinery decline with age.
- The expression of genes involved in mitochondrial/cellular homeostasis decline with age.

To address the main objective, we sampled killifish at 6, 12 and 18 weeks of age to obtain young, "middle-aged" and old killifish. We measured gene expression within tissues that are associated with age-related decline: heart, liver and skeletal muscle. We analyzed the expression of genes related to mitochondrial protein import and homeostasis (*Tomm40*, *Timm23*, *Mthsp60* and *Mthsp70*) and apoptosis (*Bcl-2*, *Bax*) by qPCR. Gene expression did not differ between the ages, however gene expression was extremely variable between samples, most notably for the 18-week time point.

4. Material and methods

4.1 Animals

Male African turquoise killifish were singly housed (two fish separated by a perforated wall in 3.8 L) at 28°C in ZebTEC Active Blue Standalone (Techniplast, Italy) aquariums at the University of Leuven. Fish were maintained on a light/dark cycle of 12h/12h. Water in the aquarium was maintained at pH 7, conductivity of 600 µs, with 15% daily exchange. Killifish larvae were fed twice daily with *Artemia salina* (Ocean Nutrition) and adults were fed twice daily with *Chironomidae* (Ocean Nutrition). Fish were not fasted before they were euthanized. Male killifish were euthanized at 6, 12 and 18 weeks of age, with a 0.5% MS-222 (tricaine methanesulfonate) overdose. They were measured and weighed (Table 5). Heart, liver, and skeletal muscle (SM) were dissected out and flash frozen in liquid nitrogen and stored at -80°C. All animal experiments were carried out in accordance to regulations of the KU Leuven Animal Ethical Committee.

4.2 Tissue homogenization

Frozen heart, liver and SM tissue were ground with mortar and pestle that was kept on dry ice to ensure that the tissue remained frozen throughout the procedure. For the 6-week time point tissue from 3 individual fish were pooled together, whereas for the 12- and 18-week time point tissue from 2 individual fish were pooled, this was to ensure an adequate starting material.

4.3 RNA extraction

For RNA extraction, approximately 50 mg tissue was homogenized in 1 ml TRIzol (Thermo Fisher Scientific, Merelbeke, Belgium) using a Potter-Elvehjem PTFE homogenizer. The homogenized solution was transferred to an Eppendorf tube and incubated at room temperature for 5 minutes, after which 0.2 ml chloroform (Merck, Overijse, Belgium) was added to each Eppendorf tube and vortexed for 15 seconds. Samples were incubated at room temperature for 3 minutes and centrifuged at 12,000 *x* g for 15 minutes at 4°C. Following

centrifugation, the upper aqueous phase was collected. To precipitate the RNA from the aqueous phase, isopropyl alcohol (Merck, Overijse, Belgium) was added at a 1:1 ratio with the aqueous phase. The samples were incubated at room temperature for 10 minutes and centrifuged at 12,000 *x* g for 10 minutes at 4°C. The supernatant was removed and the RNA pellet washed twice with 0.5 ml 75% ethanol (Merck, Overijse, Belgium) and centrifuged at 7,500 *x* g for 5 minutes at 4°C. The RNA pellet was dried and re-suspended in 25 µl of DEPC-treated water. Concentration and purity of RNA was determined using a spectrophotometer (NanoDrop, Thermo Fischer Scientific, Merelbeke, Belgium). 700 ng RNA was used for cDNA synthesis.

4.4 cDNA synthesis

cDNA was synthesized according to the manufacturers' protocol (iScript™ gDNA Clear cDNA Synthesis Kit, Bio-Rad Laboratories, Temse, Belgium). Briefly, ensure that the RNA samples were free of genomic DNA, each reaction was treated with 0.5 µl of DNase and 1.5 µl of DNase buffer and vortexed to mix. In 0.2 ml PCR tubes, RNA, water and the DNase master mix (2 µl) was vortexed. The PCR tubes were placed in a thermal cycler (Mastercycler® nexus X2 series, Eppendorf, Rotselaar, Belgium), and the following protocol was used as per the guidelines of the manufacturer (Table 1).

***Table 1*: Steps of the DNA digestion.**

DNA digestion	25	5
DNase inactivation	75	5
Storage conditions	4; ice	Until the next step

cDNA was synthesized by adding 4 µl of reverse transcription supermix to the DNase-treated RNA tubes. A control was prepared in parallel by adding supermix to the RNA sample without the addition of reverse transcriptase enzyme (no RT control). The reaction occurred in the thermal cycler as follows (Table 2):

***Table 2*: Steps of the cDNA synthesis.**

Step	Temperature, °C	Time, min
Priming	25	5
Reverse transcription	46	20
RT inactivation	95	1
Hold	4	-

Finally, reactions were diluted with DEPC-treated water at a ratio of 1:7 to achieve a concentration of 100 ng cDNA to use in the qPCR reactions.

4.5 Primer design

Primers for qPCR were designed using the following resources:

1. **Ensembl genome browser** (https://www.ensembl.org/index.html)**:** The zebrafish genome was used as a reference genome to design primers for the killifish.
2. **NCBI Nucleotide** (https://www.ncbi.nlm.nih.gov/nucleotide?cmd=search)**:** NCBI Nucleotide was used to search the nucleotide (Figure 11) and protein sequence (Figure 12) of our genes of interest (for the zebrafish, *Danio rerio*) and which were then used in a BLAST search to recover a predicted nucleotide sequence for the killifish. All the sequences were saved in the FASTA format.
3. **NCBI Blast** (https://blast.ncbi.nlm.nih.gov/Blast.cgi): The protein sequence of the zebrafish was used to find a nucleotide sequence of the mRNA in the killifish (Figure 13) (tblastn search).
4. **Pairwise Sequence Alignment** (https://www.ebi.ac.uk/Tools/psa/): This website allowed the alignment of 2 nucleotide sequences of 2 different animals (zebrafish and killifish) (Figure 15). Once the alignment was obtained, exon/intro boundaries were marked and the primers were designed.

The following are the various steps taken to design primers for the *tomm40* gene as an example.

>NM_199614.1 Danio rerio translocase of outer mitochondrial membrane 40 homolog (yeast) (tomm40), mRNA

CTGGACTGCATTGCTAAACCATGGGCAGTGTGTTGGCTGCCAGCTCCCCCAACCCACCACCAGCCTCAGG
GGGTGGCACTGCCCCGGCTGGTGCAGGTTTGGTGACAGTACCTCCAGGTTTTACTATGCCCCCGGTGTCT
GGTGTGCCACCCTCCTCGGGCACTCAGGGGCAGCCTGGAACAGACTCAGAATCCTCCCTTCCCAACCCTG
GCACATTTGAAGAATGCCATCGCAAATGCAAAGAGGTCTTCCCTGTGCAGATGGAGGGGGTTCGCTTGGT
TGTCAACAAGGGCTTGAGTAATCACTTCCAGGTTAGTCACACAATTACTCTGAGCACATTGGGGGACTCG
GGTTACAGATTTGGATCCACATATGTGGGAAGCAAGCAAACAGGACCTGCCGAGTCTTTTCCAGTCATGG
TAGGTGACATGGACAACACAGGCAGTCTAAACGCGCAGGTCATACATCAGCTCACCAACCGAGTTCGCTC
TAAAATTGCCATACAGACACAGCAACACAAGTTTGTAAACTGGCAGTGTGATGGAGAGTATCGTGGCGAT
GACTTCACAGCTGCTGTTACCCTCGGCAACCCAGATGTTCTCGTGGGATCTGGTATCCTAGTGGCGCACT
ACCTCCAGTCGTTGTCTCCCTCCTTGGTATTGGGTGGTGAGCTGGTTTACCACAAAAGGCCAGGAGAGGA
GGGCACCGTCACATCATTAGTGGGCAGATACACAGGTAGTAACTATGTCGCCACATTGACGGTTGGAGGA
GCTGGAGCACATGCATCATACTACCACAAAGCCAATGACCAGCTCCAGGTCGGGGTGGAGTTTGAGGCCA
GCACACGGATGCAGGAAACAAGCGTGTCGTTTGGTTATCAGTTGGATGTACCCAAAGCCAATCTGCTTTT
TAAAGGTTCTTTGGACAGCAACTGGGTGGTGGGAGCGACGCTGGAAAAGAAGCTGTTACCCCTTCCTCTA
TCGTTAGCTCTCGGCGCCTTCCTTAATCACCGCAAGAACAAGTTTCAGTGTGGCTTCGGCGTCACCATCG
GATAAAATGGCCATGGCCATTACAGATTCTCAACAGATACAACCCTCCGCCATGCTTGAATTGGTGCAGA
GACACGGGGACATGGACCAACACCGAAACAGACTCAGAGACTCCCAGTATTAGCGCGTTAAACCTTCACA
AAGGTGGACCAGGACAAAGAGCTCACAGGACTGTCCAACAGAGCTCTCTTCAATCTAAACGTTCAGACAG
TCATATAAGGTTTGATTTAAATAGCATACGAAAGACGTATGTCTGATATGTGCAACATTAAAGGTGTTTT
GGAAGAAAGTAGTATCTGTAATCACACTGATTTGTTTGAAAACAGTTAGCAAATGTGGTGATGCCTTTTG
TTTTTTAAGGGCAAATAATTTTTTTGGATCTGTAAACAAACCATTTATTTTGGTCTATATAAATGTGGTC
GGGTAGTTTGTGCGTGTGTTTTTTTTATGTTTTTCATTTGAGGATTTAAATGATTTAATTTTCAGTAATT
CGCTCGTCAACTGAAAATCCAATGCATGGGAAGCTCTGGGTTTGAGTGCTGGGTTGTTTAAGTCCCTTTG
TCTCATGATTATAACTTGTCACACAGAAGTGTCTGAGACTTCAGACTATGGGCTCGTTTTCCTGTATTTG
TCTTTTCGGGTCTTAGGCGCAGATTTGGGTGCTGGTTTCATAATGACCGGGCCTAACCTATCAGGCTGTC
CTTTTTATGTGTCTCGACATGAAATGCGTCACTCTGAATTTTCCACATAAAAGAATTTCCAAAGTTTGTA
TTTTAATTAGTTCTACACAGTTCAAAGGTTCTTAGGGGGCAGTCGAAAAGGGTGGATGCAGATATACTGT
AATAAACCTGTACAATTTAAACTGGTTTAAATGCCCAGAGGAGTATTTTCATGTCTCATGCTGATTTCAT
GTCGTTGTGACATGGTGGAGTACTATAAAACAGGCTTTTGGCCTGATTCTAATGGATTATTTTACAGTGC
AATTATGTTGAATAAACATTCGATTGTGAAAAAAAAAAAAAAAAAAAAAAAAA

Figure 12: **Step 1: Nucleotide sequence of *Tomm40* gene in the zebrafish.**

>NP_955908.1 mitochondrial import receptor subunit TOM40 homolog [Danio rerio]

MGSVLAASSPNPPPASGGGTAPAGAGLVTVPPGFTMPPVSGVPPSSGTQGQPGTDSESSLPNPGTFEECH
RKCKEVFPVQMEGVRLVVNKGLSNHFQVSHTITLSTLGDSGYRFGSTYVGSKQTGPAESFPVMVGDMDNT
GSLNAQVIHQLTNRVRSKIAIQTQQHKFVNWQCDGEYRGDDFTAAVTLGNPDVLVGSGILVAHYLQSLSP
SLVLGGELVYHKRPGEEGTVTSLVGRYTGSNYVATLTVGGAGAHASYYHKANDQLQVGVEFEASTRMQET
SVSFGYQLDVPKANLLFKGSLDSNWVVGATLEKKLLPLPLSLALGAFLNHRKNKFQCGFGVTIG

Figure 13: **Step 2: Protein sequence of Tom40 in the zebrafish.**

>XM_015950544.1 PREDICTED: Nothobranchius furzeri translocase of outer mitochondrial membrane 40 (tomm40), mRNA

TCGGCCAATCAGCGAACGCCATAGAGGAAATGGGCGGACATTCTAGCACTACGGTCACGGACGTTCTCGT
GAACTTTACCGGTGTTTAACTACCCCCTGGCCCCTAACCGTCTTCTCCGTTACTGTGACAGATAATGGGC
AGTGTGTTGGCTGCTGCCTCACCCAGTCCAGCCCCAGCGGCTGCTGGAGGTGGTCAAGGACTTCCAGGGT
TGGTGTCGGTCCCTCCAGGGTTCACTATGCCCTCAGTGTCTTCCGTCCCTTCAACGCCTGAATCTGGTCA
GCAGACAGATTCCTCACTCCCAAACCCAGGCACCTATGAGGAGTGCCATCGGAAATGTAAAGAGGTGTTT
CCTCTTCAGATGGAAGGAGTGCGATTGCTGGTCAACAAGGGTCTGAGTAATCACTTCCAAGTCAGTCACA
CTGTTACCCTCAGCACGCTAGGTGATTCCGGTTATCGGTTTGGTTCTACGTATGTTGGCAGTAAACAGAC
TGGACCAGCAGAGTCGTTTCCAGTCATGGTGGGAGACATGGACAACACTGGCAGTTTGAATGCTCAGATC
ATTCACCAGCTTACTAGTGCTGTACGCGCCAAAGTAGCCATCCAGACTCAGCAGCAGAAGTTCGTGAATT
GGCAGTGTGATCTGGAATATCGTGGTCAAGACTTCACCTCCGCCGTGACCCTCGGAAACCCAGATGTTCT
TGTTGGATCTGGGATTGTGGTCGCTCACTATCTCCAGTCAATCACACCATCACTGGTTTTGGGCGGAGAA
CTGGTGTATCACAGAAGACCCGGAGAGGAAGGAACAGTCACCTCCCTTTTGGGAAGGTACACAGGTGACA
ACTTTGTTGCTACTTTAACTTTGGGCGGAGCTGGAGCTCATGCTACGTACTACCACAAAGCGAATGATCA
GTTGCAGGTAGGTGTTGAATTTGAAGCCAGCACTAGGATGCAAGACACTACAACATCCTTCGGTTACCAG
CTGGACCTTCCGAAAGCTAATTTGCTCTTCAAGGGAACGGTCGACAGTAACTGGGTGGTTGGAGCTACCC
TCGAAAAGAAACTACTTCCACTCCCTCTCACGCTGGCTCTGGGGGCTTTCCTCAACCATCGCAAAAACAA
GTTTCAGTGTGGCTTCGGGGTCACCATTGGCTAGAGGTGCTCAGGCTGCCTGGAACCAGCTTTCAGACCA
CGGCTTGGACTGGCACAGAGACACAAAGGAACCTGGACTAAGTTTTAGGAATTGGATTCAGAGACTCTCT
TCCAACTGATTTCCAGGGTCAACAGAGAGACTAAGACAACTACCAAGGAGCCAGAACTGGCCGAGCCATG
CCTACATACTGTAGCACAAATGTCTTTCCTGTATGATGTTTTGGATGTACCGAGAGGTGGTGTCTATCAG
ATGGCTTCAGGTGATGCATGAGAACATGTTATGTGAAAATTAAAGTGGTACAGTAAGACATAATATATTG
TGGTCATGTATGGGTTGAAATAAATGTGATAACGTTTTGTACAACA

Figure 14: **Step 3: Predicted nucleotide sequence of *Tomm40* gene in the killifish.**

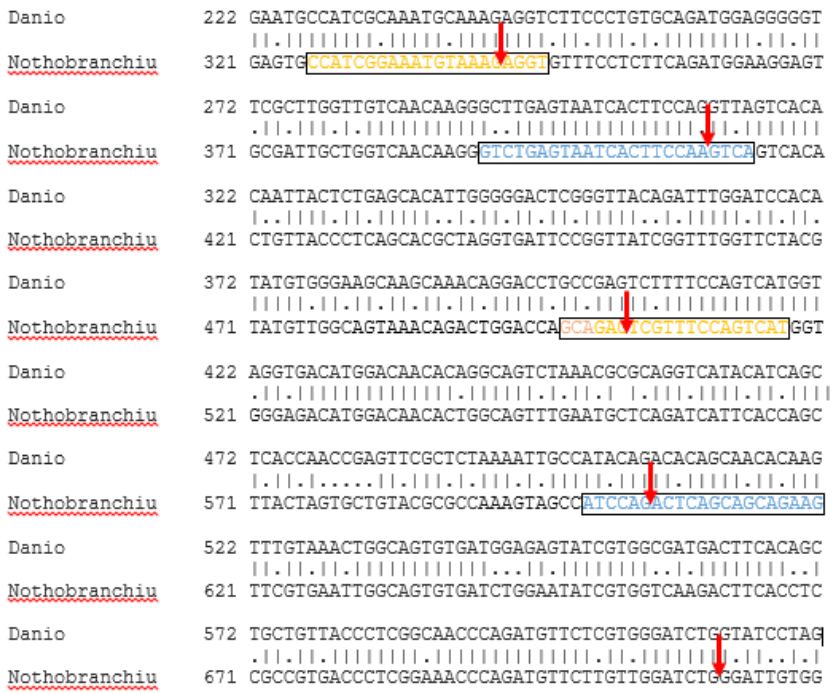

Figure 15: **Step 4: A portion of the alignment of the 2 nucleotide sequences.** The presence of a black dot between the two sequences represents different bases whereas the presence of a line between the two sequences represents similarity between the bases. The red arrows represent exon boundaries. The boxed sequences are DNA sequence in which the primers will bind. Two primer pairs are indicated by different colours. We tested both primer pairs, however we continued the experiments with only one primer pair, this decision was made by comparing the amplification plot between the two reactions.

Primers were designed over exon-exon boundaries with the exception of *Bcl*-2, due to the limited number of exon-exon boundaries while also respecting the other rules for primer design (Table 3). Primer design over exon-exon boundaries reduces the likelihood that the primers will bind and amplify genomic DNA, due the presence of introns between the exon sequences. The open-source program, Sigma Aldrich OligoEvaluator was used to calculate melting temperature, GC content and potential secondary structures. For each gene, except for *Bcl-2*, 2 pairs of primers were designed, however after testing all the primer pairs we choose the pair that resulted in the best amplification curves to move forward. For *Bax*, the both primer pairs were used in future expression measurements due to the large difference between their amplification plots. Upon further sequence analysis of the killifish genome we found that two variants exist for the Bax gene (*Baxa* and *Baxb*) (Petzold *et al*, 2013), therefore we may have designed primers that are targeting these two gene variants. We call these two primer pairs Bax(1) and Bax(2). There is currently no evidence to suggest that the other genes of interest (or reference genes) exist as multiple variants.

***Table 3*: The different primers that were designed and used for the experiments.**

Gene of interest	Forward/ Reverse	Sequence (5' to 3')	Length (bp)	Melting temperature (°C)	GC content (%)	Amplicon (bp)
Tomm40	Forward	CCATCGGAAATGTAAAGAGGT	21	61.7	42.9	147
	Reverse	ATGACTGGAAACGACTCTGC	20	61.9	50.0	
Timm23	Forward	TCCAAACCTCGTAACGTACAGATTC	25	65.9	44.0	100
	Reverse	AATGCACTGTACAACAAGAGCAAC	24	64.1	41.7	
Bcl-2 *	Forward	ATTATCGCTTTCTTCGAGTTCG	22	63.3	40.9	122
	Reverse	AAGAAGAGGACCGTTTAAATATTCC	25	62.4	36.0	
Mthsp70	Forward	AAGGAATTCAAGAGAGAGTCTGG	23	61.7	43.5	128
	Reverse	GGGAGGTTGATATCAGTCTGC	21	62.4	52.4	
Mthsp60	Forward	GACCAGAAGATCGGTGTGG	19	63.3	57.9	207
	Reverse	CGCTGTTCTCACCACCTTGG	19	63.5	57.9	
Bax (1)	Forward	TGCACTTATTGTTAAAGGACTTCATC	22	59.9	40.9	201
	Reverse	GAGAGCTTTGATGACGAGTC	20	59.2	50	
Bax (2)	Forward	AAACACAGAGCTACAAAGGATG	26	63.1	34.6	167
	Reverse	GAGAGCTTTGATGACGAGTC	22	62.1	40.9	
Gapdh*	Forward	AAAGTCGGAATCAATGGATTTGG	23	66.6	39.1	239
	Reverse	TTAGTCGGGTCCCTCTCGTG	20	66.4	60	
Actb*	Forward	CCTTCCTTCCTCGGTATGG	19	63.4	57.9	167
	Reverse	AGGTGGGGCAATGATCTTAATC	22	64.9	45.5	

**Bcl-2* is not designed over an intron-exon boundary.

**Gapdh and Actb were designed as the reference genes.

4.6 qPCR

For this step, 96-well PCR plates (Applied Biosystems by Thermo Fisher Scientific, Merelbeke, Belgium) were used. They were divided in 3 parts: 2 reference genes and 1 gene of interest; each sample was made in duplicate (Figure 16). Two negative controls were included which either contained no-RT or no cDNA template to ensure that the primers did not amplify either gDNA or a contaminant in the reaction. It was necessary to spread samples belonging to the same time points and/or tissues across several plates.

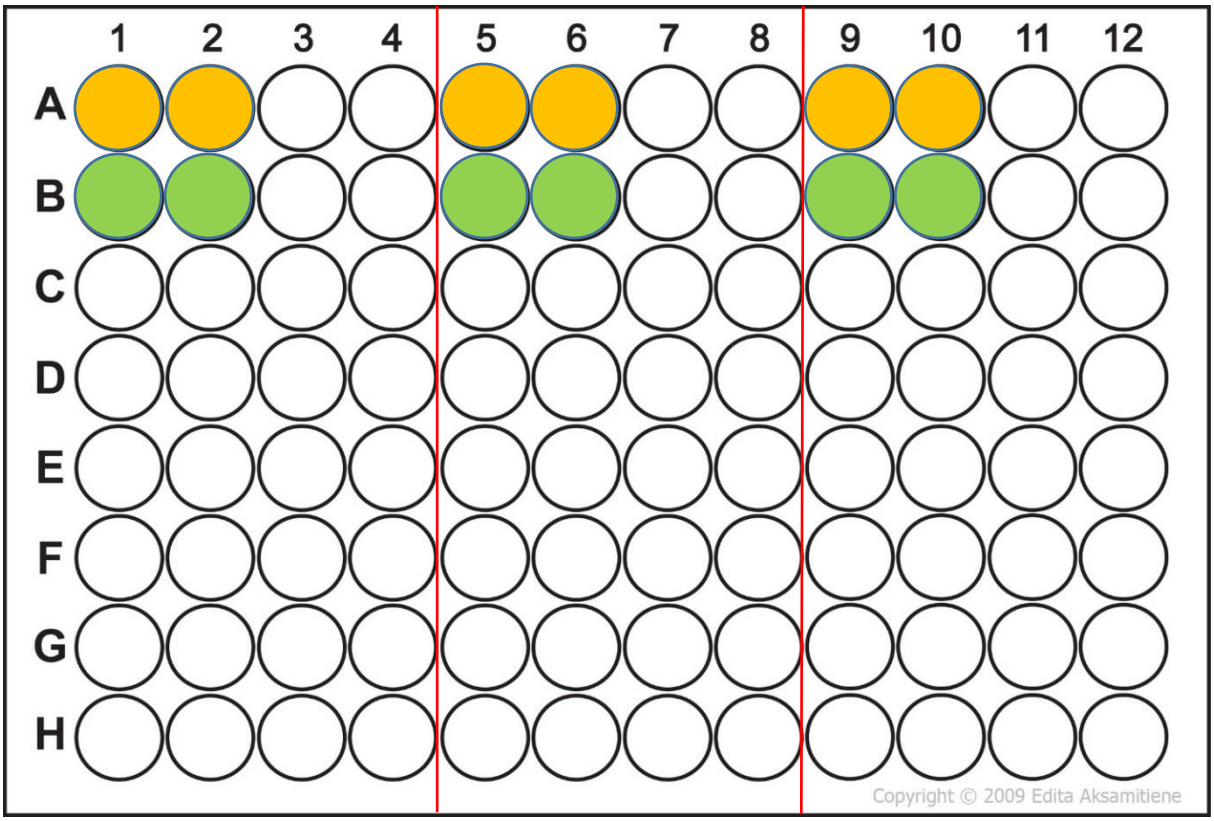

Figure 16: **Global template used for qPCR.** The red lines indicate the boundaries of the three genes tested (2 reference genes and 1 gene of interest). The circles represent the duplicates that were done on the whole plate, for example the yellow circles would be for one sample for three different genes.

A mastermix was composed of SYBR Green PCR Master Mix (Applied Biosystems by Thermo Fisher Scientific, Merelbeke, Belgium), DEPC-treated water and primers of the gene. 13 µl of the mastermix was added to each well plus 2 µl of a different sample of cDNA. Afterwards, the plate was placed in the thermal cycler and gene expression was measured (StepOnePlus Real-Time PCR System, Applied Biosystems, Merelbeke, Belgium), using the StepOne™ Software v2.3 (Table 4).

***Table 4*: Steps of the qPCR.** Cycling stage includes

Stage	Temperature, °C	Time, s
Holding stage	95	120
Cycling stage	95	15
(40 cycles)	58	15
	72	1

4.7 Agarose gel

qPCR samples were resolved on an agarose gel to confirm predicted product size. A 1.5% agarose gel was prepared by dissolving and microwaving agarose (VWR International, Oud-Heverlee, Belgium) in 1X TBE (Tris-Borate-EDTA). The gel solidified during 30 minutes at room temperature. Gel loading Dye (6X) (New England Biolabs, Evry, France) was added to the qPCR samples. The solified gel was placed in the electrophoresis unit and fully submerged in 1X TBE. A DNA molecular weight ladder (New England Biolabs, Evry, France), was loaded into the first lane of the gel and the samples were added to the other lanes. The gel was resolved for 1 hour with a voltage of 130 V. Finally, the gel was put into a solution of ethidium bromide 0.5 µg/ml with 1X TBE for 20 minutes. To visualize the qPCR products, a UV camera (Doc-Print VX5, Vilber Smart Imaging, Collégien, France) was used to take a photograph of the gel.

4.8 Statistical analysis

Statistical analysis was conducted using IBM SPSS statistics subscription (IBM Corporation, New-York, USA). Data were analyzed using univariate GLM (generalized linear model). P-values less than 0.05 were considered to be significant. Data are presented as mean + SD (Standard deviation). Gene expression measurements taken from the 18 week-time point were extremely variable, therefore we performed a student t-test between the 6- and 12-week time points.

5. Results and discussion

5.1 Lifespan curve

The lifespan of the GRZ killifish strain has been reported to range between 4 and 6 months and is easily influenced by feeding regime and laboratory setting and only recently have detailed husbandry protocols been published (Polačik *et al*, 2016; Dodzian *et al*, 2018), therefore it is common practice for individual labs to perform their own survival curves of their population of killifish. Figure 17 represents the survival curve of the killifish housed in the aqua facility at KU Leuven. It represents the percentage of survival of their fish at each week of age.

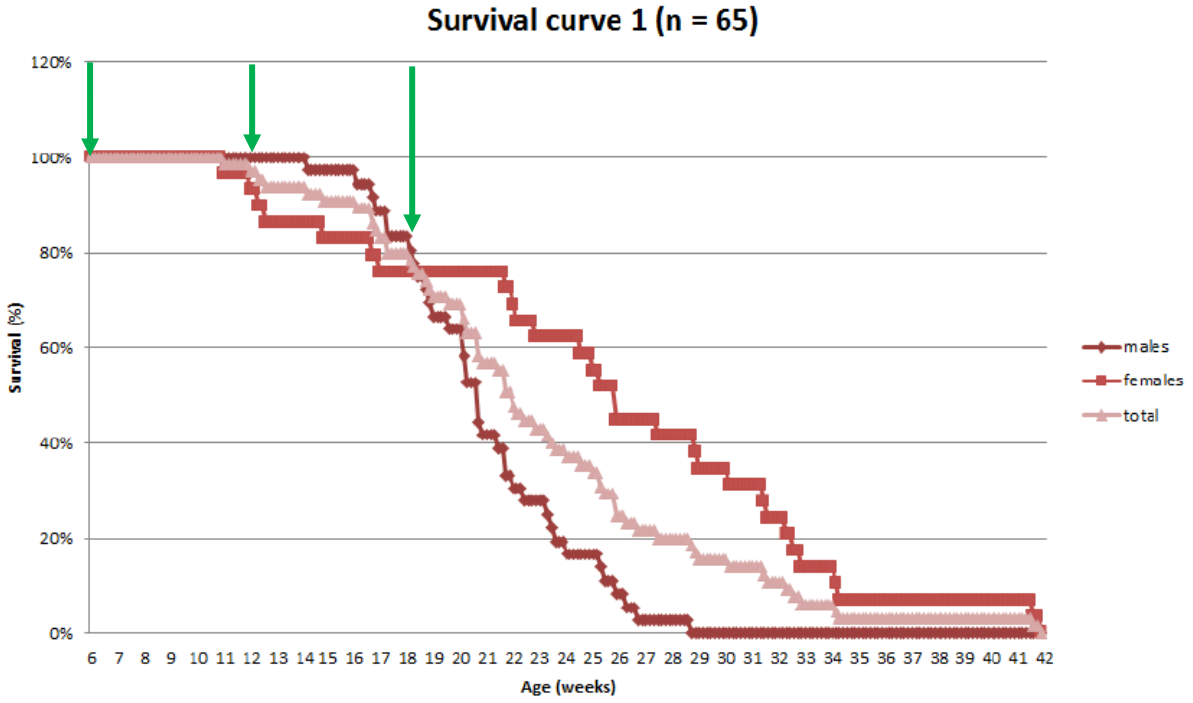

Figure 17: **Survival of a killifish population at KU Leuven.** A difference can be observed between males and females. In the present study, males were used to explore the gene expression of proteins involved in mitochondrial import and apoptosis. Green arrows represent time points in which male fish were collected.

This curve confirms the choice of the different time points. At 6 weeks, there is 100% survival, and we consider this time to include young fish. At 12 weeks, although a high percentage of survival remains, there is a noticeable divergence between female and male early mortality. At 18 weeks, female and male survival rates cross and there is a rapid decline in male survival. Although at 18 weeks, there appears to be only around 20% of mortality in the male fish, we

noted that several male fish to be used in our study did not survive until 18 weeks, and therefore we term these fish as old.

5.2 Length and body weight of the fish

Fish were measured and weighed to provide us insight into their growing rate. It should be noted that these fish were not fasted and therefore body mass may not be a reliable indicator of growth. Several fish species, including killifish grow in length over their lifespan and therefore length is a commonly used measurement to assess growth. However, as can be seen in table 5 – 7, body length is variable in these male fish.

***Table 5*: Body mass and body length of fish at 6 weeks of age (young).** Tissues from three individual fish were pooled together to generate one sample. Body length is measured from snout/mouth to end of tail fin.

ID – Number of the fish	Mass, g	Length, cm
KF#1A	0.29	
KF#2A	0.55	
KF#3A	0.75	
KF#4A	0.50	
KF#5A	0.64	
KF#6A	0.76	
KF#7A	0.68	
KF#8A	1.06	4.3
KF#9A	1.35	4.3
KF#10A	1.44	5.0
KF#11A	1.13	4.5
KF#12A	1.38	4.6
KF#13A	1.32	5.0
KF#14A	1.47	4.7
KF#15A	0.89	4.0
KF#16A	1.24	4.3
KF#17A	1.13	4.2
KF#18A	1.13	4.4
Mean	0.98	4.48
SD	0.36	0.32

***Table 6*: Body mass and body length of fish at 12 weeks of age (middle-aged).** Tissues from two individual fish were pooled together to generate one sample. Body length is measured from snout/mouth to end of tail fin.

ID – Number of the fish	Mass, g	Length, cm
KF#1B	2.90	
KF#2B	2.49	
KF#3B	2.09	
KF#4B	2.28	5.3
KF#5B	2.86	6.0
KF#6B	3.24	6.2
KF#7B	2.26	5.6
KF#8B	2.53	5.7
KF#9B	2.28	5.7
KF#10B	2.43	6.0
KF#11B	2.26	5.6
KF#12B		5.9
Mean	2.51	5.77
SD	0.35	0.27

***Table 7*: Body mass and body length of fish at 18 weeks of age (old).** Tissues from two individual fish were pooled together to generate one sample. Body length is measured from snout/mouth to end of tail fin.

ID – Number of the fish	Mass, g	Length, cm
KF#1C		
KF#2C	3.70	6.5
KF#3C	3.10	6.0
KF#4C	1.44	4.8
KF#5C	2.53	5.8
KF#6C	3.55	6.3
KF#7C	2.65	6.0
KF#8C	2.26	5.5
KF#9C	2.68	5.8
KF#10C	3.49	6.0
Mean	2.82	5.85
SD	0.72	0.49

Mean body mass and mean body length (from Table 5 to 7) increase with age (Figure 18). There is a greater increase in both body mass and length between 6 weeks and 12 weeks compared to the time between 12 weeks and 18 weeks. Statistical analysis showed that the body mass and the body length were significantly different between 6 and 12 weeks (p-value < 0.05) as well as between 6 and 18 weeks (p-value < 0.05) but not between 12 and 18 weeks (p-value = 0.310/p-value = 0.896).

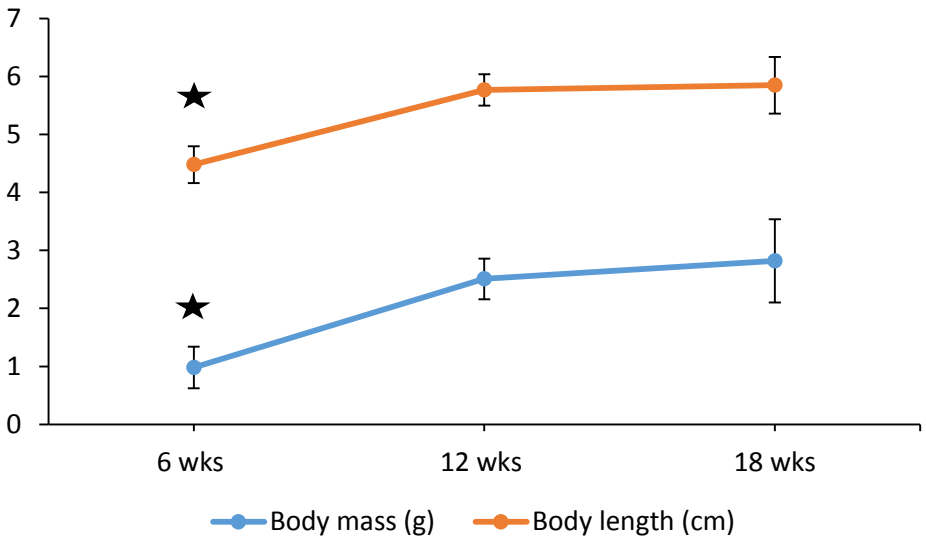

Figure 18: **Evolution of body mass and body length with age.** Univariate GLM was used for the statistical analysis and a post hoc test was used to know the signification between the means of the different time points. The six week time point is significantly different in both cases (star).

5.3 Purity and concentration of RNA extraction

The concentration of RNA was measured with a spectrophotometer in addition to assess purity of the RNA, two absorbance ratios were measured. The A260/A280 represents the level of purity of the RNA, a value of 2 represents pure RNA, free from phenol and/or proteins that absorb at 280nm. In contrast, the A260/A230 is a secondary measurement of nucleic acid purity, and a value between 2-2.2 represents a pure sample (Technologies, 2007). Values that are lower than this may indicate contaminants that absorb at 230, for example TRIzol absorbs at both 230 and 270.

***Table 8*: Purity and concentration of extracted RNA in liver samples.** A: fish of 6 weeks of age (young). B: fish of 12 weeks of age (middle-aged). C: fish of 18 weeks of age (old). These concentrations were further diluted for cDNA synthesis.

N° of the sample	A260/A280	A260/A230	Concentration, ng/µl
1A	2.02	1.09	1948.8
2A	2.04	1.22	1846.3
3A	2.03	1.57	2584.7
4A	2.02	1.64	2386.5
5A	1.99	1.19	1339.5
6A	1.99	0.60	1732.8
Mean 6 weeks	**2.015**	**1.218**	**1973.10**
1B	2.00	1.26	3783.2
2B	2.03	1.49	2110.8
3B	1.97	1.13	1411.5
4B	2.01	1.33	1078.3
5B	2.04	1.24	1435.6
6B	2.02	1.57	3198.0
Mean 12 weeks	**2.012**	**1.337**	**2169.57**
1C	2.00	1.38	1283.1
2C	1.96	0.95	1435.5
3C	1.99	1.42	881.2
4C	2.00	1.49	1338.0
5C	1.88	1.32	1475.8
Mean 18 weeks	**1.966**	**1.312**	**1282.72**

***Table 9*: Purity and concentration of extracted RNA in the skeletal muscle samples.**
A: fish of 6 weeks of age (young). B: fish of 12 weeks of age (middle-aged). C: fish of 18 weeks of age (old).

N° of the sample	A260/A280	A260/A230	Concentration, ng/µl
1A	2.02	0.87	360.4
2A	2.07	1.61	756.6
3A	1.96	1.45	382.2
4A	1.99	1.21	431.2
5A	1.92	1.01	331.6
6A	2.02	1.46	531.7
Mean 6 weeks	**1.997**	**1.268**	**465.62**
1B	2.06	1.61	693.7
2B	2.07	1.84	625.8
3B	2.01	2.01	649.8
4B	2.06	1.65	413.5
5B	2.08	1.75	483.8
6B	1.98	1.73	219.1
Mean 12 weeks	**2.043**	**1.765**	**514.28**
1C	1.99	0.90	506.6
2C	2.05	1.39	954.0
3C	2.08	1.70	542.7
4C	2.03	1.43	1051.0
5C	1.69	0.81	282.6
Mean 18 weeks	**1.968**	**1.246**	**667.38**

***Table 10*: Purity and concentration of extracted RNA in the heart samples.** A: fish of 6 weeks of age (young). B: fish of 12 weeks of age (middle-aged). C: fish of 18 weeks of age (old).

N° of the sample	A260/A280	A260/A230	Concentration, ng/µl
1A	2.01	1.30	353.7
2A	1.95	0.72	352.4
3A	1.97	1.98	391.6
4A	2.00	0.98	565.3
5A	1.88	1.51	167.5
6A	1.89	1.37	355.8
Mean 6 weeks	**1.950**	**1.310**	**364.38**
1B	2.02	1.56	488.8
2B	1.82	1.90	105.2
3B	2.04	2.06	846.3
4B	2.04	2.06	535.2
5B	2.00	1.94	483.8
6B	2.08	2.07	767.8
Mean 12 weeks	**2.000**	**1.931**	**587.85**
1C	2.07	1.82	982.2
2C	1.94	1.44	278.1
3C	1.96	1.10	681.0
4C	1.89	1.28	381.3
5C	1.87	1.34	477.6
Mean 18 weeks	**1.946**	**1.396**	**560.04**

RNA that was isolated from liver, skeletal muscle (SM) and heart tissue have A260/A280 ratios that are near 2, indicating these samples are relatively free from contaminants, such as some phenols and proteins that absorb at 280 nm. In contrast, the ratio A260/A230, was lower than 2, although this indicates contamination most likely due to the use of TRIzol, there is no indication that this impacted the quality of cDNA that was synthesized from this RNA. TRIzol extraction does not rely on a column for purification and this may be why we have a lower

A260/A230 ratio, however the use of this method allowed us to recover high amounts of RNA. In the future, it is likely not required to pool samples together to obtain sufficient starting material of RNA to be used in cDNA synthesis.

5.4 Amplification curve and melting curve

The amplification plot that we obtain measuring gene expression with qPCR (Figure 19) displays the number of cycles required before there is noticeable doubling of the qPCR product. It gives us a cycle threshold (Ct) value, which represents the first cycle from which the machine detects amplification. If this value is high, the amplification, and thus the expression, is low and vice versa. Mthsp60 (Figure 19) has a Ct value between 23 and 29 for a threshold of 0.1 (Table 11). The other amplification plots for the remaining genes can be found in the Annex.

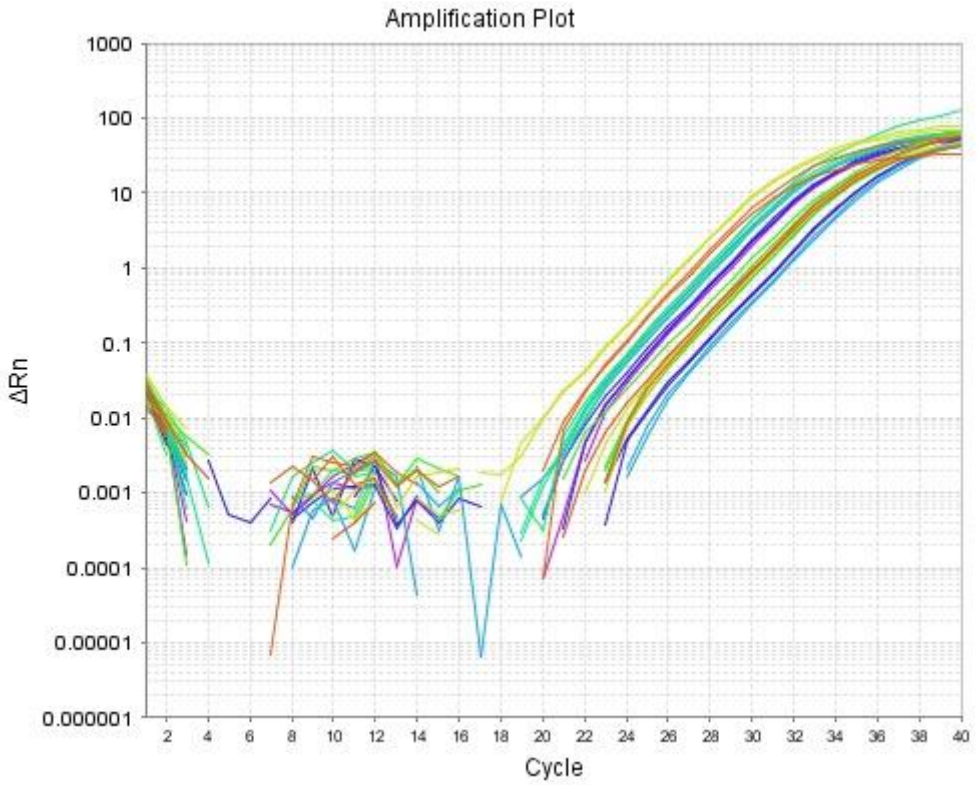

Figure 19: **Amplification plot of gene *mthsp60*.** The number of cycles needed to amplify the product is between 23 and 29 for a threshold of 0.1. Rn value represents the fluorescent signal from SYBR Green normalized to the signal of the passive reference dye (ROX). ΔRn represents the experimental Rn value minus the Rn value of the baseline signal generated by the instrument. Concretely, it calculates the magnitude of the specific signal generated from a given set of PCR conditions.

In addition to amplification curves, another output from the StepOnePlus Real-Time PCR System is a melting curve (Figure 20), this can be used as a quality control to confirm that only one product is amplified during the qPCR and therefore can be used to indicate the selectivity of the primer pair. Only one peak was noted for the melting curve for mthsp60 (Figure 20). The melting curves for the remaining genes can be found in the Annex and also only have one peak each.

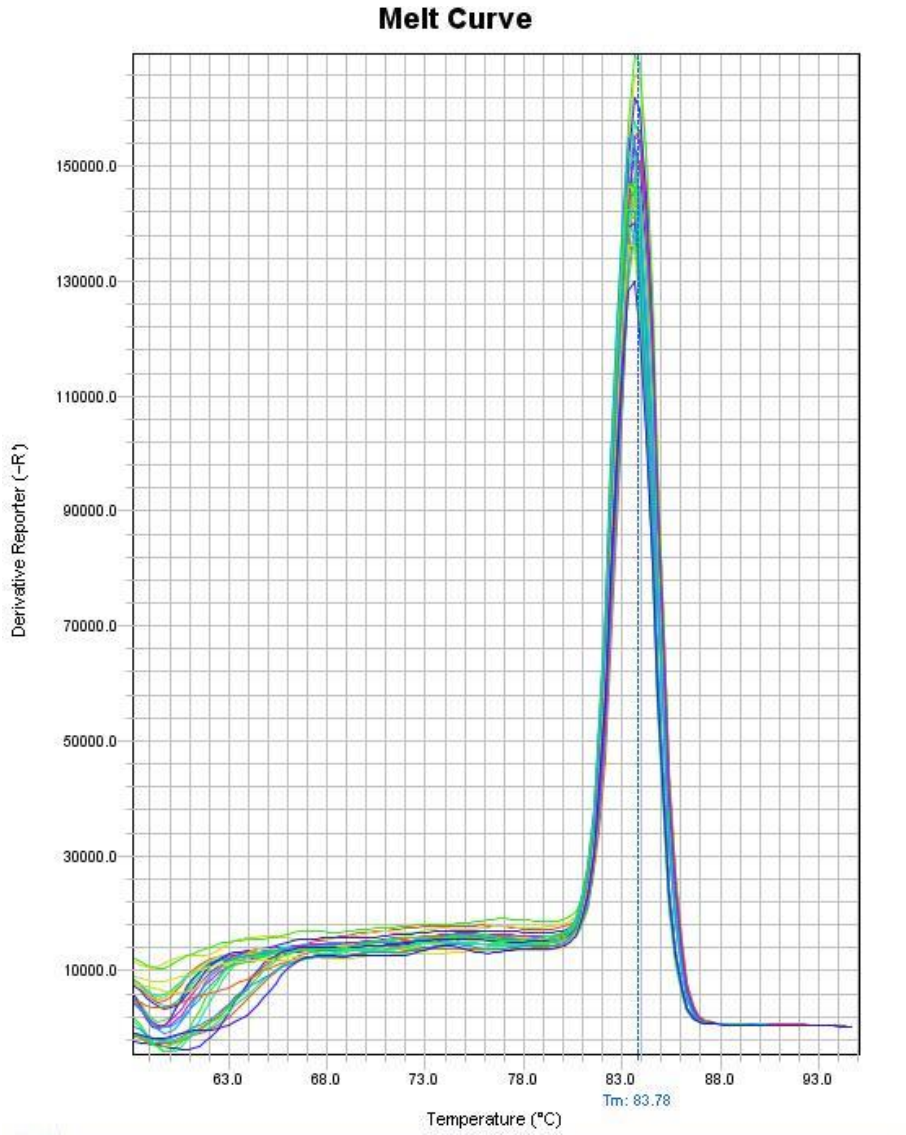

Figure 20: **Melting curve of gene *mthsp60*.** It is a quality control because it confirms the amplification of only 1 product.

Table 11: **Ct values of the different genes.**

Genes	Ct values (threshold of 0.1)
Tomm40	27-31
Timm23	28-33
Mthsp60	23-29
Mthsp70	24-31
Bcl-2	32-39
Bax(1)	32-37
Bax(2)	28-33
Actb	21-27
Gapdh	18-23

5.5 Agarose gel

qPCR product for each gene of interest was resolved on an agarose gel to confirm the results of the melting curve, that only one product was generated with the designed primer pair (Figure 21). The approximate sizes of qPCR product coincided with the predicted product size in Table 12. The predicted size and the approximate size are very close for each PCR product, confirming that the primers were specific and that the correct product was amplified. There were exceptions with *Tomm40* and *Bax1*. The genome of the killifish has only recently been sequenced, and several of the primers were designed using predicted gene sequences, which along with the gene may contain other functional elements such as regulatory regions. Furthermore, there may be gene variants that have yet to be identified. This may explain the differences between the predicted size and the approximate size for tom40. In the case of Bax, there is evidence that two variants exist (Petzold *et al*, 2013). The predicted size was calculated from the Sigma Aldrich OligoEvaluator online program.

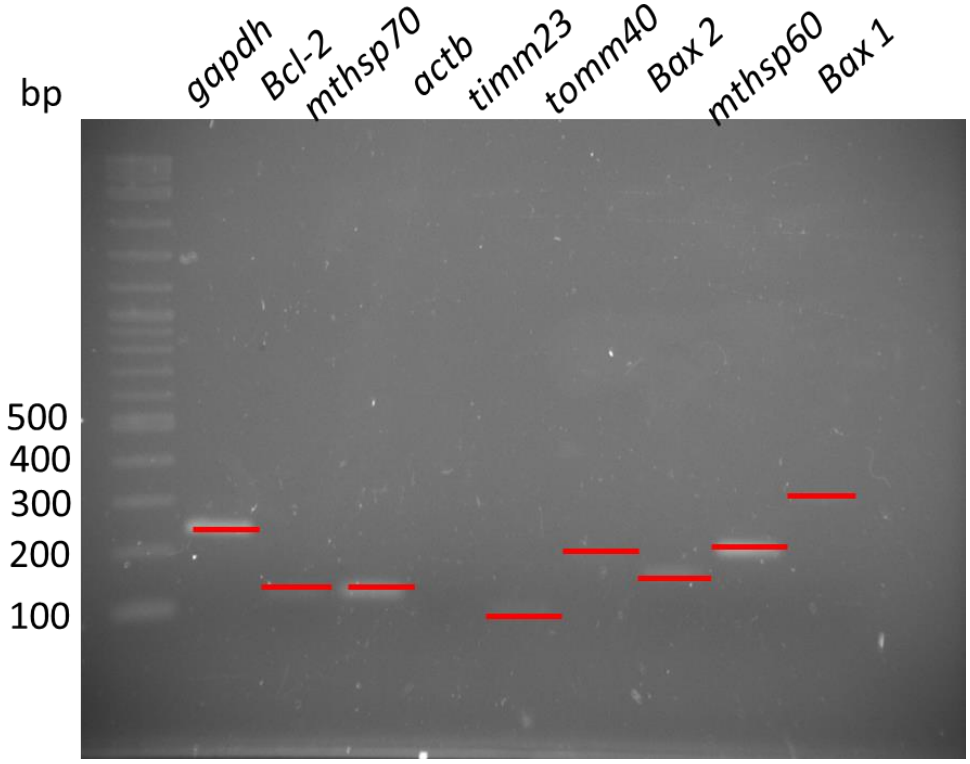

Figure 21: **Agarose gel.** 2-log DNA New England Biolabs Ladder is used to know the size of the products. For *Actb*, we can't observe the product. This can be due to a manipulation error. Red lines have been added to improve visibility. The size of the products is relatively similar to the predicted sizes.

Table 12**: Predicted and approximate sizes of the amplified products.**

Gene	Predicted size (bp)	Approximate size (gel) (bp)
Gapdh	239	240
Bcl-2	122	120
Mthsp70	128	125
Actb	167	/
Timm23	100	100
Tomm40	147	190
Bax 2	167	160
Mthsp60	207	200
Bax 1	201	300

5.6 Gene expression

Gene expression did not differ between 6-, 12- or 18-weeks (Figure 22 – 28). The SD is very high, suggesting a large variability within the samples. In particular, we noticed that the 18-week measurements differed in some cases by more than 10-fold. Age alone at 18 weeks may explain the variability at this age, for example at this time male fish are considered old and some are in the late stage of their life. Therefore, their physiological state can be very different from one fish to another, and this can explain a part of the variability in the gene expression. However, gene expression did not differ when t-tests were run to test differences between the two earlier time points. The p-values can be find in Annex 3.

The overall variability was also likely influenced by the reference gene amplification. Although *Gapdh* and *Actb* are routinely used as reference genes we realized that expression of these two genes did not remain stable within or between samples over the timepoints selected. The expression of *Gapdh* differed more so than *Actb* therefore it was removed from the data analysis. Furthermore, plate variability was observed between samples of one gene of interest, which increased the global variability. The low sample number may have also contributed to the lack of significance and in some cases the sample number was lower than 6 due to the removal of extreme measurements. A detailed literature search did not reveal any studies regarding gene expression of *Timm23* and *Tomm40* during the normal progression of ageing. However, there is evidence to suggest that protein level of Tom22, a TOM receptor protein, does not change between young and old mice (Joseph *et al*, 2013), in addition mitochondrial fractions in old mice appear to be enriched for Tom40 and Tom22 (Joseph *et al*, 2010).

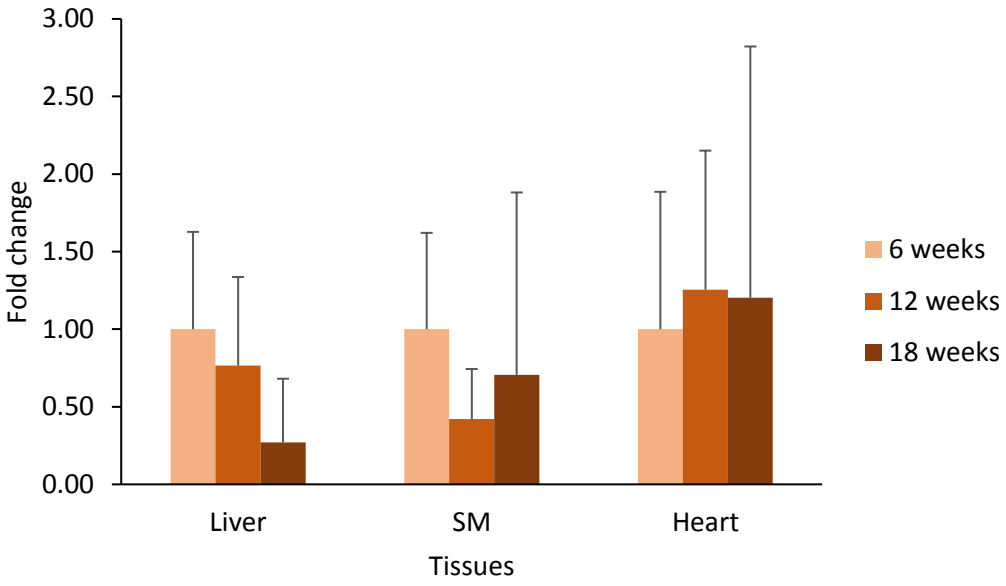

Figure 22: **Comparison of the gene expression of *Tomm40,* with age, in liver, skeletal muscle (SM) and heart.** 6 weeks is considered as the reference (=1). Overall, N is equal to 6 for 6 and 12 week time points and equal to 5 for the 18 week time point.

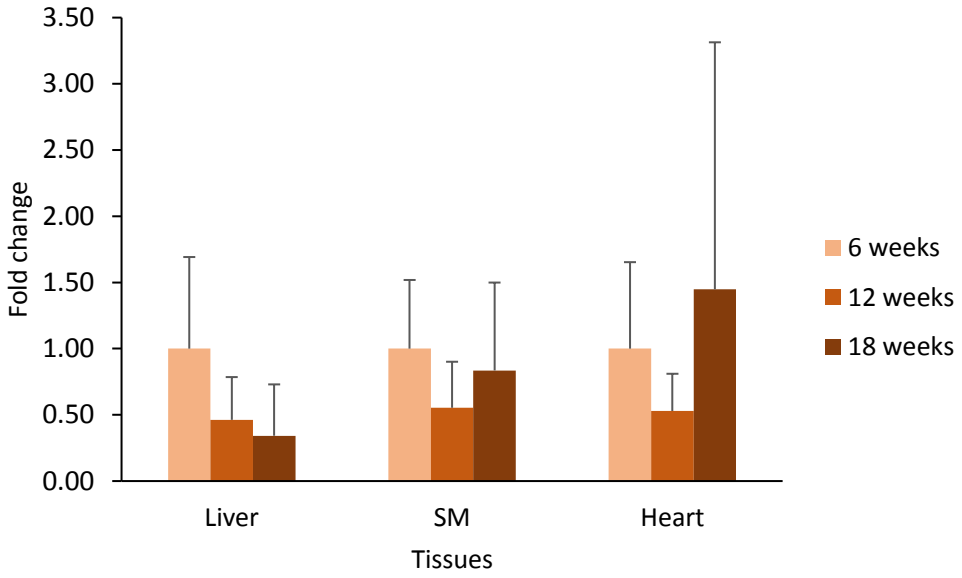

Figure 23: **Comparison of the gene expression of *Timm23,* with age, in liver, skeletal muscle (SM) and heart.** 6 weeks is considered as the reference (=1). Overall, N is equal to 6 for 6 and 12 week time points and equal to 5 for the 18 week time point.

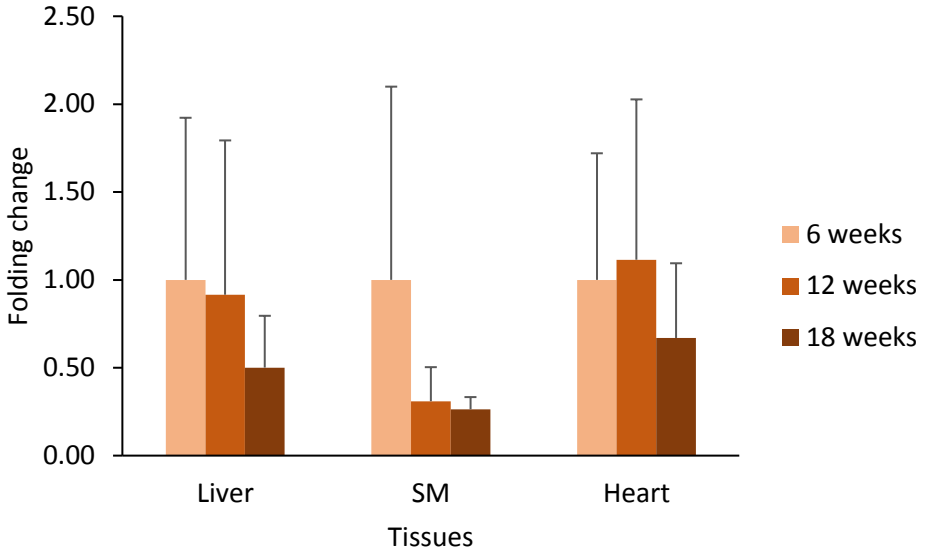

Figure 24: **Comparison of the gene expression of *Mthsp60,* with age, in liver, skeletal muscle (SM) and heart.** 6 weeks is considered as the reference (=1). Overall, N is equal to 6 for 6 and 12 week time points and equal to 5 for the 18 week time point.

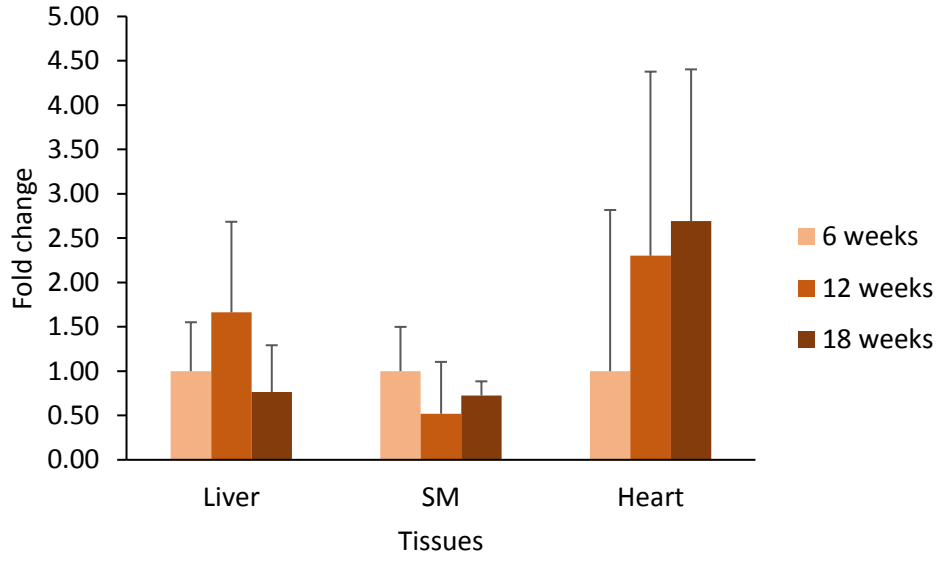

Figure 25: **Comparison of the gene expression of *Mthsp70,* with age, in liver, skeletal muscle (SM) and heart.** 6 weeks is considered as the reference (=1). Overall, N is equal to 6 for 6 and 12 week time points and equal to 5 for the 18 week time point.

We did not observe any difference in gene expression of *Mthsp70* and *Mthsp60* with age in the killifish. Multiple sequence alignment has indicated that HSP are highly homologous between various species, suggesting a conservation of their activity (Yang *et al*, 2014). Previous evidence suggests a decline in the gene expression of Hsp70, with age in the Rotifer *Brachionus calyciflorus Pallas* and the reduction in gene expression inversely correlated with the accumulation of damaged proteins in the cell (Yang *et al*, 2014). HSP synthesis has been

reported to decline in neuronal cells and muscle cells (reviewed in Murshid *et al*, 2013) and lifespan of Drosophila can be extended by overexpressing Hsp22 (Morrow *et al*, 2004), suggesting the importance of HSP in ageing and lifespan. Furthermore, plasma levels of Hsp60 correlate with an increased incidence of age-related cardiovascular disease (Pockley *et al*, 2000), in contrast, plasma levels of Hsp70 have been shown to be inversely correlated with lifespan in centenarians (Terry *et al*, 2006). It is unclear why this difference occurs and if it is specific to certain HSP, it may also be necessary to compare the correlation of protein level and/or activity in tissue extracts in addition to the plasma levels, as proteins in the plasma may or may not have activity.

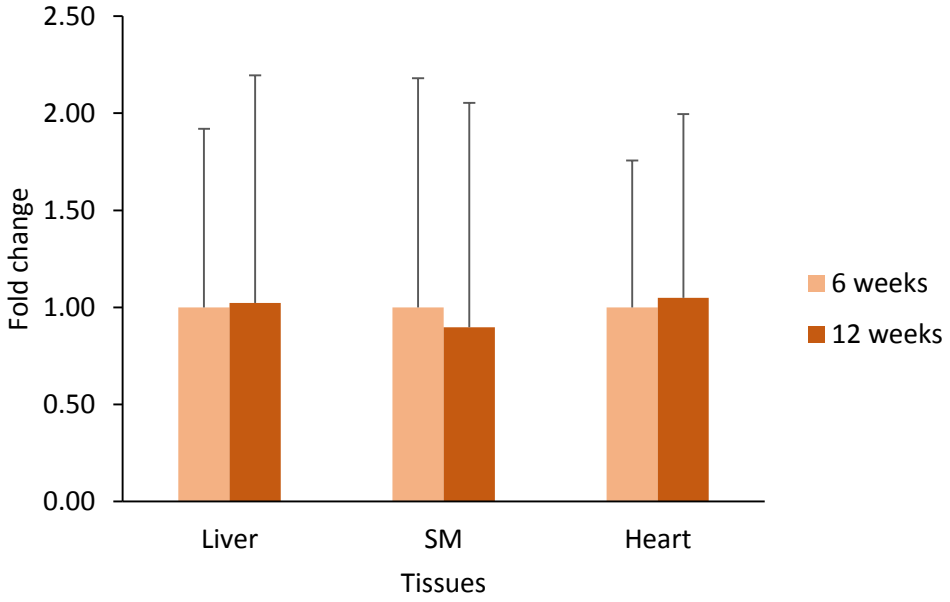

Figure 26: **Comparison of the gene expression of *Bcl-2,* with age, in liver, skeletal muscle (SM) and heart.** 6 weeks is considered as the reference (=1). Overall, N is equal to 6 for 6 and 12 week time points and equal to 5 for the 18 week time point. The 18 week time has not been represented because the values were too variable and so it had no sense to put them on the graph.

We found that *Bcl-2* gene expression did not differ between 6 and 12 week old fish. Measurements from 18 week old fish were removed due to a too high variability between the samples, it had no sense to put them on the graph. Previous studies reported reduced gene and protein expression of Bcl-2 in T cells isolated from blood sampled from older individuals compared to younger individuals (Aggarwal & Gupta, 1998). Although Bcl-2 expression is reduced in T cells of older individuals, there is also evidence to suggest that Bcl-2 expression

may not correlate with ageing. For example, mice null for *Bcl-2* do not show clear signs of ageing although approximately 50% die by 6 weeks of age (Nakayama *et al*, 1994). In addition, senescent cells in culture are unable to down-regulate Bcl-2 expression in response to apoptosis-inducing stimuli (Wang *et al*, 1994) (REF). Senescent cells are believed to accumulate during aging.

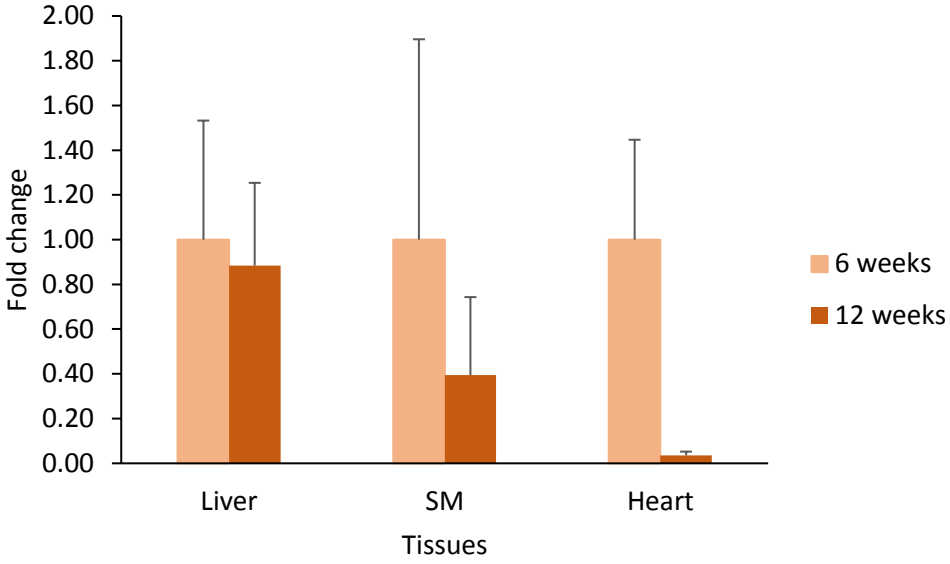

Figure 27: **Comparison of the gene expression of *Bax(1),* with age, in liver, skeletal muscle (SM) and heart.** 6 weeks is considered as the reference (=1). Overall, N is equal to 6 for 6 and 12 week time points and equal to 5 for the 18 week time point. The 18 week time has not been represented because the values were too variable and so it had no sense to put them on the graph.

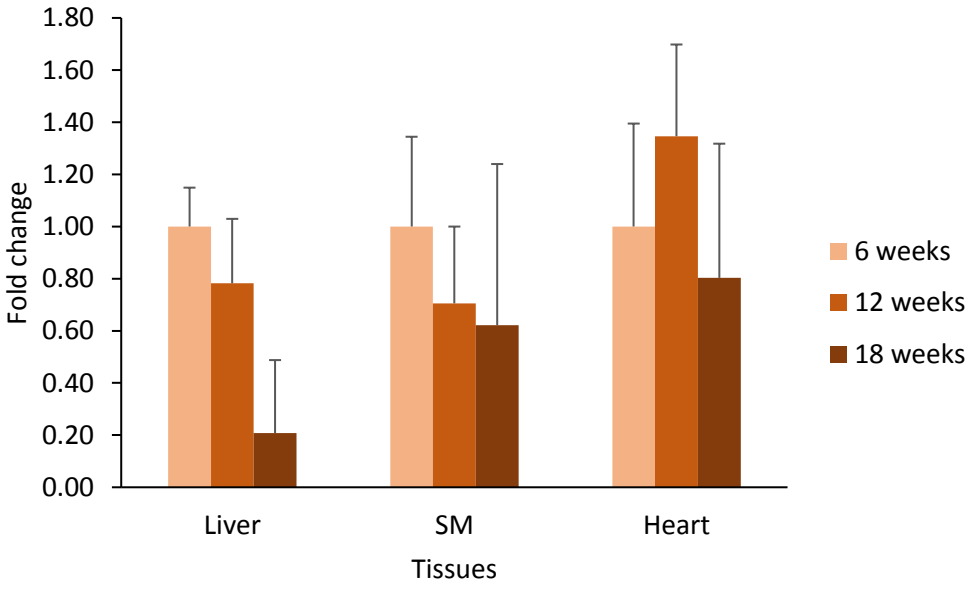

Figure 28: **Comparison of the gene expression of *Bax(2),* with age, in liver, skeletal muscle (SM) and heart.** 6 weeks is considered as the reference (=1). Overall, N is equal to 6 for 6 and 12 week time points and equal to 5 for the 18 week time point.

Bax expression levels was lower at 18-weeks of age in the liver, however this did not reach significance. Bax gene expression within colon tissue extracts has been reported to remain unchanged with age in male rats (Lee *et al*, 2000). Bax loss-of-function reduces age-related health problems but does not extend lifespan (Perez *et al*, 2007). Together, this suggests that a reduction in Bax may improve health however it may not slow ageing.

6. Conclusions and perspectives

This master thesis investigated expression of genes involved in mitochondria homeostasis; genes involved in mitochondrial protein import and apoptosis pathways in the African Turquoise Killifish, a new model for ageing studies.

For this aim, tissues (liver, skeletal muscle and heart) were collected from male fish from the fish facilities of KU Leuven. Tissues were pooled together to form samples and RNA was extracted from these samples using TRIzol. cDNA was synthetized from this RNA and used to measure gene expression using qPCR technologies. To achieve this, primers were designed for 7 genes of interest (*Tomm40*, *Timm23*, *Mthsp60*, *Mthsp70*, *Bcl-2*, *Bax(1)*, *Bax(2)*) and for 2 reference genes (*Gapdh*, *Actb*).

Specificity of the primers were validated by melting curves calculated from the StepOnePlus Real-Time PCR System program and by product size resolved on an agarose gel. The melting curves revealed one peak, suggesting the amplification of only one product while the agarose gel showed that the sizes of the amplified products were approximately equal to the predicted sizes.

Gene expression appeared highly variable and overall gene expression did not differ between any time points, although there was a trend for gene expression to decrease with age in the liver tissue. It is recommended to repeat some of these measurements, however first to ensure that a reference gene is found that does not change expression level with age, such genes as tbp (TATA-box binding protein), hprt1 (hypoxanthine guanine phosphoribosyl transferase) and ef-1 (elongation factor 1), will be measured. If their expression is stable, they could be use as housekeeping genes for qPCR.

In addition, the number of samples may have been low due to the decision to pool samples together, however we know for future experiments that we likely do not have to pool samples together for at least liver, SM and heart tissue extracts. It may also be better to increase the number of fish in an attempt to reduce the variability.

Finally, we noticed a plate-to-plate variability; in the future we will attempt to minimize this by loading the samples of one tissue on one plate. We can also include a standard curve in each plate and calculate expression relative to the curve.

This thesis was only the beginning of a large field of research about ageing, a lot of things are still to study but the main objective of these experiments was to try to understand better how we age. Although we did not see any difference in gene expression the work included in this thesis provided us insight into how to improve gene expression measurements.

7. Bibliography

Aggarwal S & Gupta S (1998) Ligand, Bcl-2, and Bax Humans: Altered Expression of Fas (CD95), Fas Increased Apoptosis of T Cell Subsets in Aging Available at: http://www.jimmunol.org/content/160/4/http://www.jimmunol.org/content/160/4/1627.full#ref-list-1 [Accessed August 11, 2018]

Ahting U, Floss T, Uez N, Schneider-Lohmar I, Becker L, Kling E, Iuso A, Bender A, de Angelis MH, Gailus-Durner V, Fuchs H, Meitinger T, Wurst W, Prokisch H & Klopstock T (2009) Neurological phenotype and reduced lifespan in heterozygous Tim23 knockout mice, the first mouse model of defective mitochondrial import. *Biochim. Biophys. Acta - Bioenerg.* **1787:** 371–376

Birben E, Sahiner UM, Sackesen C, Erzurum S & Kalayci O (2012) Oxidative stress and antioxidant defense. *World Allergy Organ. J.* **5:** 9–19 Available at: http://www.ncbi.nlm.nih.gov/pubmed/23268465 [Accessed May 24, 2018]

Bobkova N V., Evgen'ev M, Garbuz DG, Kulikov AM, Morozov A, Samokhin A, Velmeshev D, Medvinskaya N, Nesterova I, Pollock A & Nudler E (2015) Exogenous Hsp70 delays senescence and improves cognitive function in aging mice. *Proc. Natl. Acad. Sci.* **112:** 16006–16011 Available at: http://www.ncbi.nlm.nih.gov/pubmed/26668376 [Accessed August 6, 2018]

Bratic A & Larsson NG (2013) The role of mitochondria in aging. *J. Clin. Invest.* **123:** 951–957 Available at: http://www.ncbi.nlm.nih.gov/pubmed/23454757 [Accessed November 18, 2017]

Brown KA, Didion SP, Andresen JJ & Faraci FM (2007) Effect of aging, MnSOD deficiency, and genetic background on endothelial function: Evidence for MnSOD haploinsufficiency. *Arterioscler. Thromb. Vasc. Biol.* **27:** 1941–1946

Bürkle A, Moreno-Villanueva M, Bernhard J, Blasco M, Zondag G, Hoeijmakers JHJ, Toussaint O, Grubeck-Loebenstein B, Mocchegiani E, Collino S, Gonos ES, Sikora E, Gradinaru D, Dollé M, Salmon M, Kristensen P, Griffiths HR, Libert C, Grune T, Breusing N, et al (2015)

MARK-AGE biomarkers of ageing. *Mech. Ageing Dev.* **151:** 2–12 Available at: http://dx.doi.org/10.1016/j.mad.2015.03.006 [Accessed October 4, 2017]

Campos JC, Bozi LHM, Bechara LRG, Lima VM & Ferreira JCB (2016) Mitochondrial Quality Control in Cardiac Diseases. *Front. Physiol.* **7:** 479 Available at: http://journal.frontiersin.org/article/10.3389/fphys.2016.00479/full [Accessed May 9, 2018]

Cui H, Kong Y & Zhang H (2012) Oxidative stress, mitochondrial dysfunction, and aging. *J. Signal Transduct.* **2012:** 646354 Available at: http://www.ncbi.nlm.nih.gov/pubmed/21977319 [Accessed August 6, 2018]

Curran SP, Leverich EP, Koehler CM & Larsen PL (2004) Defective Mitochondrial Protein Translocation Precludes Normal *Caenorhabditis elegans* Development. *J. Biol. Chem.* **279:** 54655–54662 Available at: http://www.ncbi.nlm.nih.gov/pubmed/15485840 [Accessed August 6, 2018]

Davies M (2016) The global elderly explosion: Number of old people is rising faster than ever and will DOUBLE in 30 years | Daily Mail Online. Available at: http://www.dailymail.co.uk/health/article-3513167/Global-elderly-population-exploding-US-report.html [Accessed May 9, 2018]

Devi L, Prabhu BM, Galati DF, Avadhani NG & Anandatheerthavarada HK (2006) Accumulation of amyloid precursor protein in the mitochondrial import channels of human Alzheimer's disease brain is associated with mitochondrial dysfunction. *J. Neurosci.* **26:** 9057–68 Available at: http://www.jneurosci.org/cgi/doi/10.1523/JNEUROSCI.1469-06.2006 [Accessed May 24, 2018]

Diekert K, Kispal G, Guiard B & Lill R (1999) An internal targeting signal directing proteins into the mitochondrial intermembrane space. *Proc. Natl. Acad. Sci. U. S. A.* **96:** 11752–7 Available at: http://www.ncbi.nlm.nih.gov/pubmed/10518522 [Accessed July 25, 2018]

Dodzian J, Kean S, Seidel J & Valenzano DR (2018) A Protocol for Laboratory Housing of Turquoise Killifish (Nothobranchius furzeri). *J. Vis. Exp.* Available at: http://www.ncbi.nlm.nih.gov/pubmed/29708537 [Accessed August 16, 2018]

Dudek J, Rehling P & van der Laan M (2013) Mitochondrial protein import: Common principles and physiological networks. *Biochim. Biophys. Acta - Mol. Cell Res.* **1833:** 274–285 Available at: https://www.sciencedirect.com/science/article/pii/S0167488912001449 [Accessed July 25, 2018]

Elmore S (2007) Apoptosis: A Review of Programmed Cell Death. *Toxicol. Pathol.* **35:** 495–516 Available at: http://www.ncbi.nlm.nih.gov/pubmed/17562483 [Accessed October 7, 2017]

Gilkerson RW, Selker JML & Capaldi RA (2003) The cristal membrane of mitochondria is the principal site of oxidative phosphorylation. *FEBS Lett.* **546:** 355–358 Available at: https://www.sciencedirect.com/science/article/pii/S0014579303006331 [Accessed May 24, 2018]

Giorgi C, Agnoletto C, Bononi A, Bonora M, De Marchi E, Marchi S, Missiroli S, Patergnani S, Poletti F, Rimessi A, Suski JM, Wieckowski MR & Pinton P (2012) Mitochondrial calcium homeostasis as potential target for mitochondrial medicine. *Mitochondrion* **12:** 77–85 Available at: http://www.ncbi.nlm.nih.gov/pubmed/21798374 [Accessed May 24, 2018]

Gómez-Serrano M, Camafeita E, López JA, Rubio MA, Bretón I, García-Consuegra I, García-Santos E, Lago J, Sánchez-Pernaute A, Torres A, Vázquez J & Peral B (2016) Differential proteomic and oxidative profiles unveil dysfunctional protein import to adipocyte mitochondria in obesity-associated aging and diabetes. *Redox Biol.* **11:** 415–428 Available at: https://www.sciencedirect.com/science/article/pii/S2213231716303457 [Accessed May 24, 2018]

Harel I, Valenzano DR & Brunet A (2016) Efficient genome engineering approaches for the short-lived African turquoise killifish. *Nat. Protoc.* **XI:** 2010–2028 Available at: http://www.nature.com/doifinder/10.1038/nprot.2016.103

Herrmann JM, Stuart RA, Craig EA & Neupert W (1994) Mitochondrial heat shock protein 70, a molecular chaperone for proteins encoded by mitochondrial DNA. *J. Cell Biol.* **127:** 893–902 Available at: http://www.ncbi.nlm.nih.gov/pubmed/7962074 [Accessed May 24, 2018]

Joseph A-M, Adhihetty PJ, Wawrzyniak NR, Wohlgemuth SE, Picca A, Kujoth GC, Prolla TA & Leeuwenburgh C (2013) Dysregulation of Mitochondrial Quality Control Processes Contribute to Sarcopenia in a Mouse Model of Premature Aging. *PLoS One* **8:** e69327 Available at: http://www.ncbi.nlm.nih.gov/pubmed/23935986 [Accessed August 16, 2018]

Joseph A-M, Ljubicic V, Adhihetty PJ & Hood DA (2010) Biogenesis of the mitochondrial Tom40 channel in skeletal muscle from aged animals and its adaptability to chronic contractile activity. *Am. J. Physiol. Physiol.* **298:** C1308–C1314 Available at: http://www.ncbi.nlm.nih.gov/pubmed/20107041 [Accessed August 16, 2018]

Kim Y, Nam HG & Valenzano DR (2016) The short-lived African turquoise killifish: an emerging experimental model for ageing. *Dis. Model. Mech.* **IX:** 115–129 Available at: http://www.ncbi.nlm.nih.gov/pubmed/26839399 [Accessed September 28, 2017]

Kumazaki T, Sasaki M, Nishiyama M, Teranishi Y, Sumida H & Mitsui Y (2002) Effect of BCL-2 down-regulation on cellular life span. *Biogerontology* **3:** 291–300 Available at: http://link.springer.com/10.1023/A:1020170517755 [Accessed August 7, 2018]

Leak RK (2014) Heat shock proteins in neurodegenerative disorders and aging. *J. Cell Commun. Signal.* **8:** 293–310 Available at: http://www.ncbi.nlm.nih.gov/pubmed/25208934 [Accessed May 24, 2018]

Lee H-M, Greeley GH & Englander EW (2000) Effects of aging on expression of genes involved in regulation of proliferation and apoptosis in the colonic epithelium. *Mech. Ageing Dev.* **115:** 139–155 Available at: https://www.sciencedirect.com/science/article/pii/S0047637400001202 [Accessed August 11, 2018]

Limón-Pacheco J & Gonsebatt ME (2009) The role of antioxidants and antioxidant-related enzymes in protective responses to environmentally induced oxidative stress. *Mutat. Res. Toxicol. Environ. Mutagen.* **674:** 137–147 Available at: https://www.sciencedirect.com/science/article/pii/S1383571808002714 [Accessed May 9, 2018]

Lindsay J, Esposti MD & Gilmore AP (2011) Bcl-2 proteins and mitochondria—Specificity in

membrane targeting for death. *Biochim. Biophys. Acta - Mol. Cell Res.* **1813:** 532–539 Available at: https://www.sciencedirect.com/science/article/pii/S0167488910002831 [Accessed May 11, 2018]

Lithgow T & Schneider A (2010) Evolution of macromolecular import pathways in mitochondria, hydrogenosomes and mitosomes. *Philos. Trans. R. Soc. Lond. B. Biol. Sci.* **365:** 799–817 Available at: http://www.ncbi.nlm.nih.gov/pubmed/20124346 [Accessed May 9, 2018]

Logan DC (2007) The mitochondrial compartment. *J. Exp. Bot.* **58:** 1225–43 Available at: http://www.ncbi.nlm.nih.gov/pubmed/17269154 [Accessed May 24, 2018]

Di Maio R, Barrett PJ, Hoffman EK, Barrett CW, Zharikov A, Borah A, Hu X, McCoy J, Chu CT, Burton EA, Hastings TG & Greenamyre JT (2016) α-Synuclein binds to TOM20 and inhibits mitochondrial protein import in Parkinson's disease. *Sci. Transl. Med.* **8:** 342ra78-342ra78 Available at: http://www.ncbi.nlm.nih.gov/pubmed/27280685 [Accessed May 9, 2018]

Matsuyama S, Palmer J, Bates A, Poventud-Fuentes I, Wong K, Ngo J & Matsuyama M (2016) Bax-induced apoptosis shortens the life span of DNA repair defect Ku70-knockout mice by inducing emphysema. *Exp. Biol. Med.* **241:** 1265–1271 Available at: http://www.ncbi.nlm.nih.gov/pubmed/27302174 [Accessed August 7, 2018]

McIlwain DR, Berger T & Mak TW (2013) Caspase functions in cell death and disease. *Cold Spring Harb. Perspect. Biol.* **5:** 1–28 Available at: http://www.ncbi.nlm.nih.gov/pubmed/23545416 [Accessed November 18, 2017]

Morrow G, Samson M, Michaud S & Tanguay RM (2004) Overexpression of the small mitochondrial Hsp22 extends Drosophila life span and increases resistance to oxidative stress. *FASEB J.* **18:** 598–599 Available at: http://www.ncbi.nlm.nih.gov/pubmed/14734639 [Accessed August 16, 2018]

Murshid A, Eguchi T & Calderwood SK (2013) Stress proteins in aging and life span. *Int. J. Hyperthermia* **29:** 442–7 Available at: http://www.ncbi.nlm.nih.gov/pubmed/23742046 [Accessed August 16, 2018]

Nakayama K, Nakayama K, Negishi I, Kuida K, Sawa H & Loh DY (1994) Targeted disruption of

Bcl-2 alpha beta in mice: occurrence of gray hair, polycystic kidney disease, and lymphocytopenia. *Proc. Natl. Acad. Sci. U. S. A.* **91:** 3700–4 Available at: http://www.ncbi.nlm.nih.gov/pubmed/8170972 [Accessed August 16, 2018]

Nicholls DG, Ferguson SJ, Nicholls DG & Ferguson SJ (2013) Respiratory Chains. *Bioenergetics***:** 91–157 Available at: https://www.sciencedirect.com/science/article/pii/B9780123884251000051 [Accessed August 7, 2018]

Parcellier A, Gurbuxani S, Schmitt E, Solary E & Garrido C (2003) Heat shock proteins, cellular chaperones that modulate mitochondrial cell death pathways. *Biochem. Biophys. Res. Commun.* **304:** 505–512 Available at: https://www.sciencedirect.com/science/article/pii/S0006291X03006235 [Accessed February 7, 2018]

Perez GI, Jurisicova A, Wise L, Lipina T, Kanisek M, Bechard A, Takai Y, Hunt P, Roder J, Grynpas M & Tilly JL (2007) Absence of the proapoptotic Bax protein extends fertility and alleviates age-related health complications in female mice. *Proc. Natl. Acad. Sci. U. S. A.* **104:** 5229–34 Available at: http://www.ncbi.nlm.nih.gov/pubmed/17360389 [Accessed August 16, 2018]

Petzold A, Reichwald K, Groth M, Taudien S, Hartmann N, Priebe S, Shagin D, Englert C & Platzer M (2013) The transcript catalogue of the short-lived fish Nothobranchius furzeri provides insights into age-dependent changes of mRNA levels. *BMC Genomics* **14:** 185 Available at: http://www.ncbi.nlm.nih.gov/pubmed/23496936 [Accessed August 16, 2018]

Pockley AG, Wu R, Lemne C, Kiessling R, de Faire U & Frostegård J (2000) Circulating heat shock protein 60 is associated with early cardiovascular disease. *Hypertens. (Dallas, Tex. 1979)* **36:** 303–7 Available at: http://www.ncbi.nlm.nih.gov/pubmed/10948094 [Accessed August 16, 2018]

Polačik M, Blažek R & Reichard M (2016) Laboratory breeding of the short-lived annual killifish Nothobranchius furzeri. *Nat. Protoc.* **11:** 1396–1413 Available at: http://www.ncbi.nlm.nih.gov/pubmed/27388556 [Accessed August 16, 2018]

Ray PD, Huang B-W & Tsuji Y (2012) Reactive oxygen species (ROS) homeostasis and redox regulation in cellular signaling. *Cell. Signal.* **24:** 981–90 Available at: http://www.ncbi.nlm.nih.gov/pubmed/22286106 [Accessed May 24, 2018]

Renehan AG, Booth C & Potten CS (2001) What is apoptosis, and why is it important? *BMJ* **322:** 1536–8 Available at: http://www.ncbi.nlm.nih.gov/pubmed/11420279 [Accessed October 2, 2017]

Rose MR, Flatt T, Graves JL, Greer LF, Martinez DE, Matos M, Mueller LD, Shmookler Reis RJ & Shahrestani P (2012) What is aging? *Front. Genet.* **3:** 134 Available at: http://www.ncbi.nlm.nih.gov/pubmed/22833755 [Accessed November 7, 2017]

Shi Y (2004) Caspase activation, inhibition, and reactivation: A mechanistic view. *Protein Sci.* **13:** 1979–1987 Available at: http://www.ncbi.nlm.nih.gov/pubmed/15273300 [Accessed November 18, 2017]

Smith A, AF Parkes M, K Atkin-Smith G, Tixeira R, KH Poon I & Poon I (2017) Cell disassembly during apoptosis. *WikiJournal Med.* **4:** 8 Available at: https://en.wikiversity.org/wiki/WikiJournal_of_Medicine/Cell_disassembly_during_apoptosis [Accessed August 7, 2018]

Smith J (2012) Role of Krebs Cycle and ATP Production in ME/CFS. Available at: https://phoenixrising.me/archives/14280 [Accessed May 24, 2018]

Technologies N (2007) T e c h n i c a l s u p p o r t b u l l e t i n t009 260/280. **:** 8–9

Terry DF, Wyszynski DF, Nolan VG, Atzmon G, Schoenhofen EA, Pennington JY, Andersen SL, Wilcox MA, Farrer LA, Barzilai N, Baldwin CT & Asea A (2006) Serum heat shock protein 70 level as a biomarker of exceptional longevity. *Mech. Ageing Dev.* **127:** 862–868 Available at: http://www.ncbi.nlm.nih.gov/pubmed/17027907 [Accessed August 16, 2018]

Terzibasi E, Valenzano DR, Benedetti M, Roncaglia P, Cattaneo A, Domenici L & Cellerino A (2008) Large differences in aging phenotype between strains of the short-lived annual fish Nothobranchius furzeri. *PLoS One* **3:** e3866 Available at: http://www.ncbi.nlm.nih.gov/pubmed/19052641 [Accessed May 11, 2018]

Trifunovic A & Larsson N-G (2008a) Mitochondrial dysfunction as a cause of ageing. *J. Intern. Med.* **263:** 167–178 Available at: http://doi.wiley.com/10.1111/j.1365-2796.2007.01905.x [Accessed February 14, 2018]

Trifunovic A & Larsson NG (2008b) Mitochondrial dysfunction as a cause of ageing. *J. Intern. Med.* **263:** 167–178

Tsujimoto Y (1998) Role of Bcl-2 family proteins in apoptosis: Apoptosomes or mitochondria? *Genes to Cells* **3:** 697–707 Available at: http://doi.wiley.com/10.1046/j.1365-2443.1998.00223.x [Accessed November 18, 2017]

United Nations Les personnes âgées | Nations Unies. Available at: http://www.un.org/fr/sections/issues-depth/ageing/index.html [Accessed May 24, 2018]

University of Helsinki Mitochondrial dysfunction is the root cause of many diseases -- ScienceDaily. *Mitochondrial Dysfunct. is root cause many Dis.* Available at: https://www.sciencedaily.com/releases/2017/01/170126093255.htm [Accessed July 25, 2018]

Valenzano DR, Aboobaker A, Seluanov A & Gorbunova V (2017) Non-canonical aging model systems and why we need them. *EMBO J.* **XXXVI:** 959–963 Available at: http://emboj.embopress.org/lookup/doi/10.15252/embj.201796837

Valenzano DR, Benayoun BA, Singh PP, Zhang E, Etter PD, Hu C-K, Clément-Ziza M, Willemsen D, Cui R, Harel I, Machado BE, Yee M-C, Sharp SC, Bustamante CD, Beyer A, Johnson EA & Brunet A (2015) The African Turquoise Killifish Genome Provides Insights into Evolution and Genetic Architecture of Lifespan. *Cell* **163:** 1539–54 Available at: http://www.ncbi.nlm.nih.gov/pubmed/26638078 [Accessed July 25, 2018]

Wang C & Youle RJ (2009) The Role of Mitochondria in Apoptosis. *Annu. Rev. Genet.* **43:** 95–118 Available at: http://www.annualreviews.org/doi/10.1146/annurev-genet-102108-134850

Wang E, Lee M-J & Pandey S (1994) Control of fibroblast senescence and activation of programmed cell death. *J. Cell. Biochem.* **54:** 432–439 Available at:

http://www.ncbi.nlm.nih.gov/pubmed/8014192 [Accessed August 16, 2018]

Warner HR (1997) Aging and regulation of apoptosis. *Curr. Top. Cell. Regul.* **35:** 107–121 Available at: http://www.ncbi.nlm.nih.gov/pubmed/9192177 [Accessed November 18, 2017]

Wiedemann N & Pfanner N (2017) Mitochondrial Machineries for Protein Import and Assembly. *Annu. Rev. Biochem.* **86:** 685–714 Available at: https://doi.org/10.1146/annurev-biochem-060815-014352 [Accessed November 18, 2017]

Yang J, Mu Y, Dong S, Jiang Q & Yang J (2014) Changes in the expression of four heat shock proteins during the aging process in Brachionus calyciflorus (rotifera). *Cell Stress Chaperones* **19:** 33–52 Available at: http://link.springer.com/10.1007/s12192-013-0432-0 [Accessed August 11, 2018]

Annex

Annex 1: Amplification plots

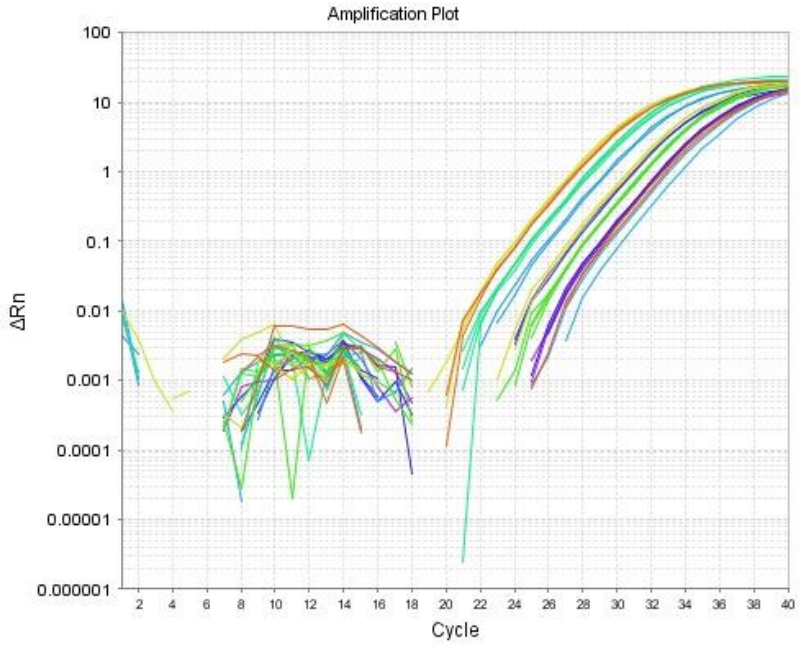

Amplification plot of gene *mthsp70*.

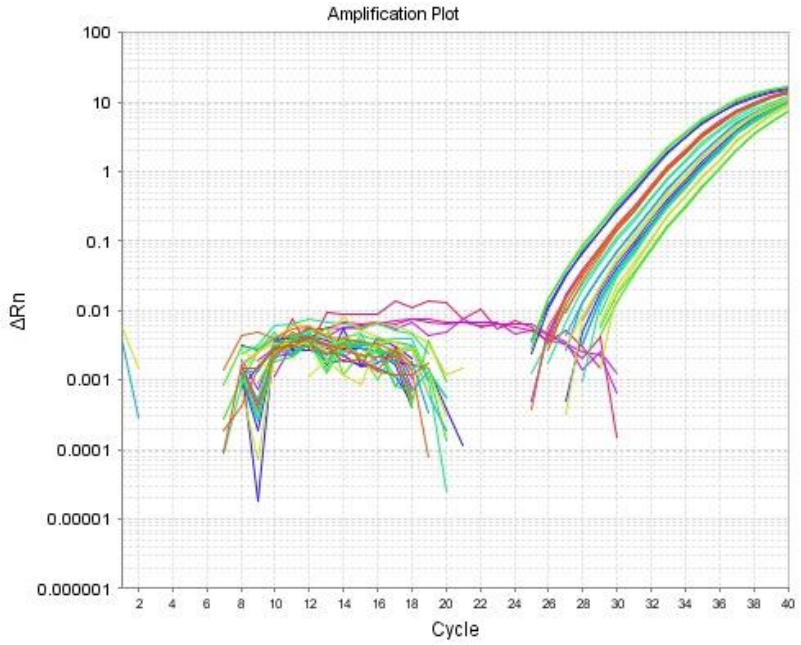

Amplification plot of gene *timm23*.

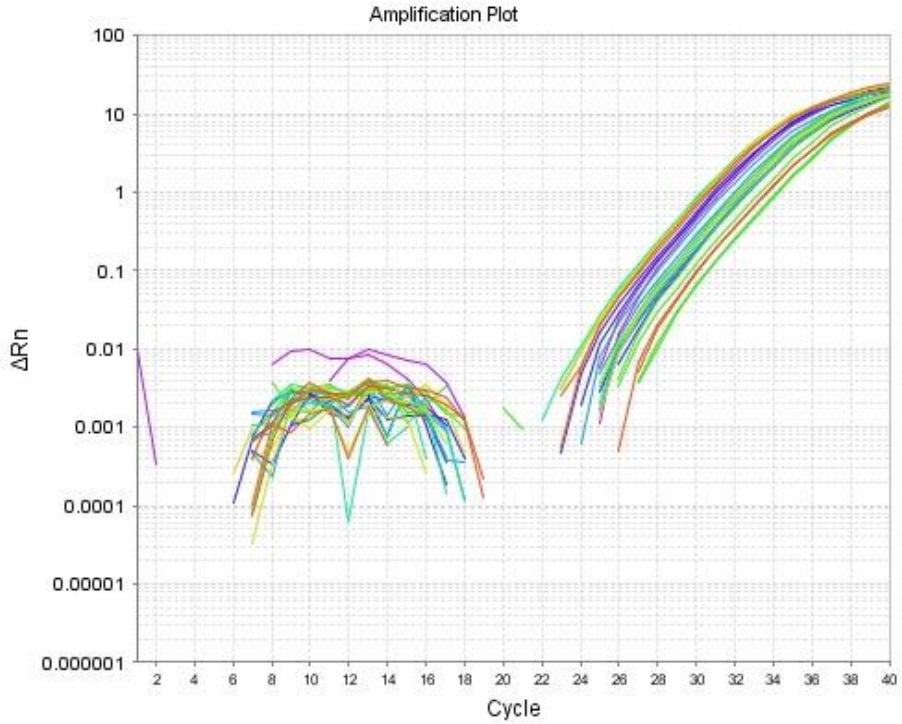

Amplification plot of gene *tomm40*.

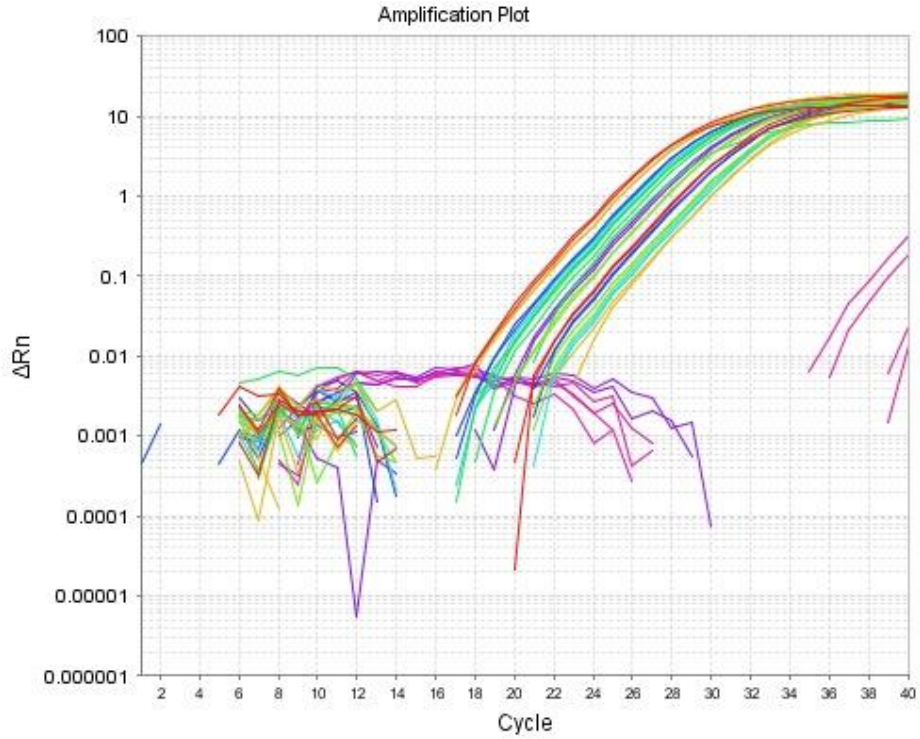

Amplification plot of gene *Actb.*

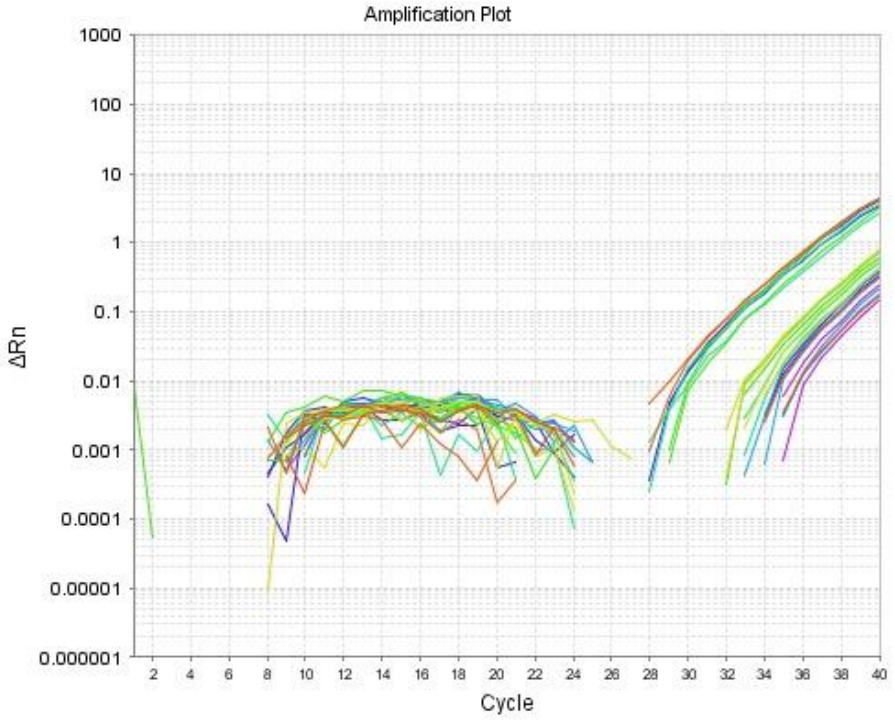

Amplification plot of gene *Bcl-2*.

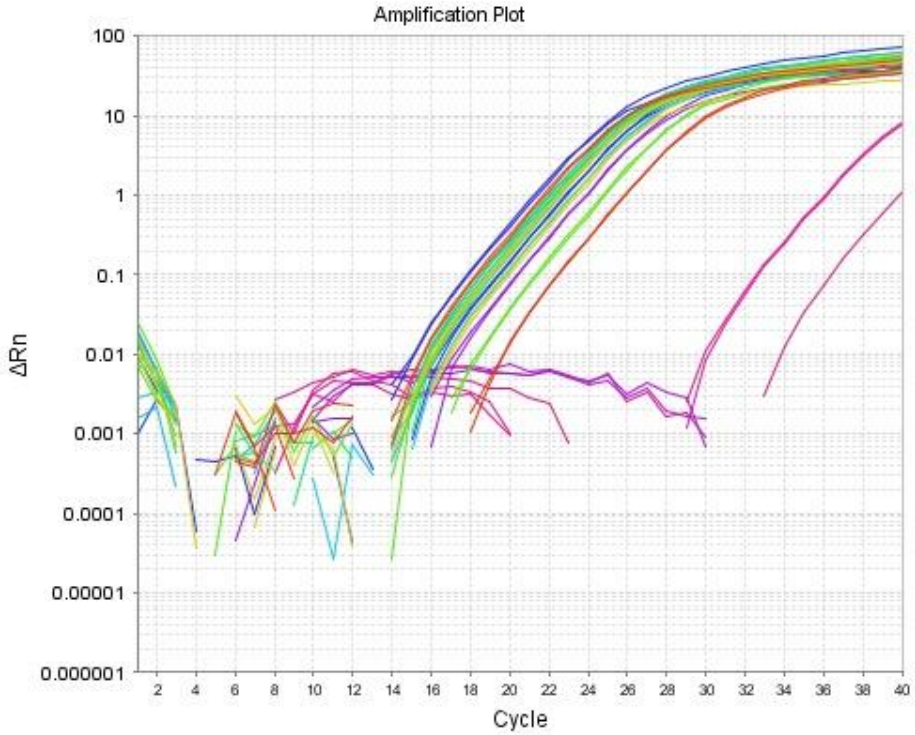

Amplification plot of gene *Gapdh*.

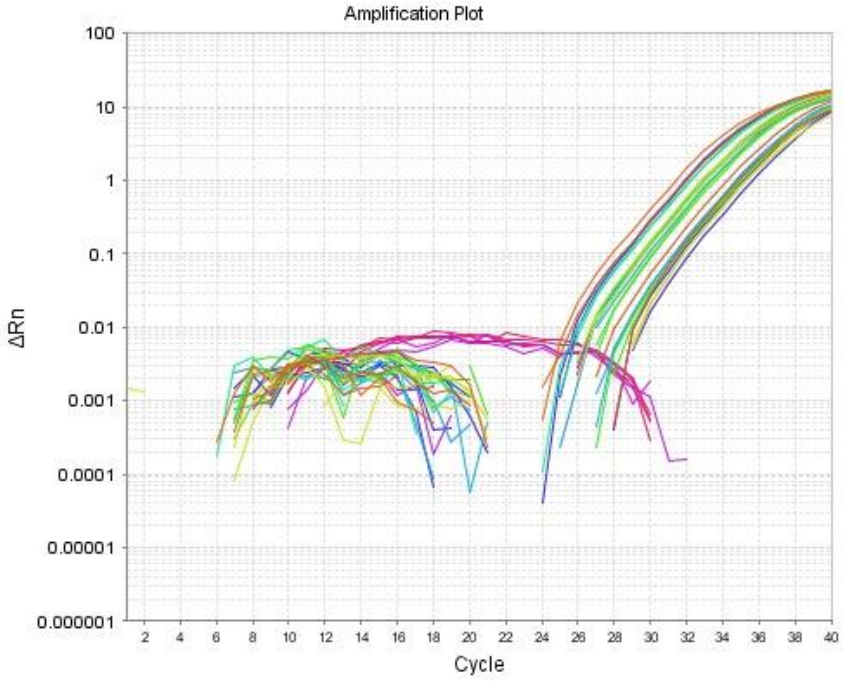

Amplification plot of gene *Bax(2)*.

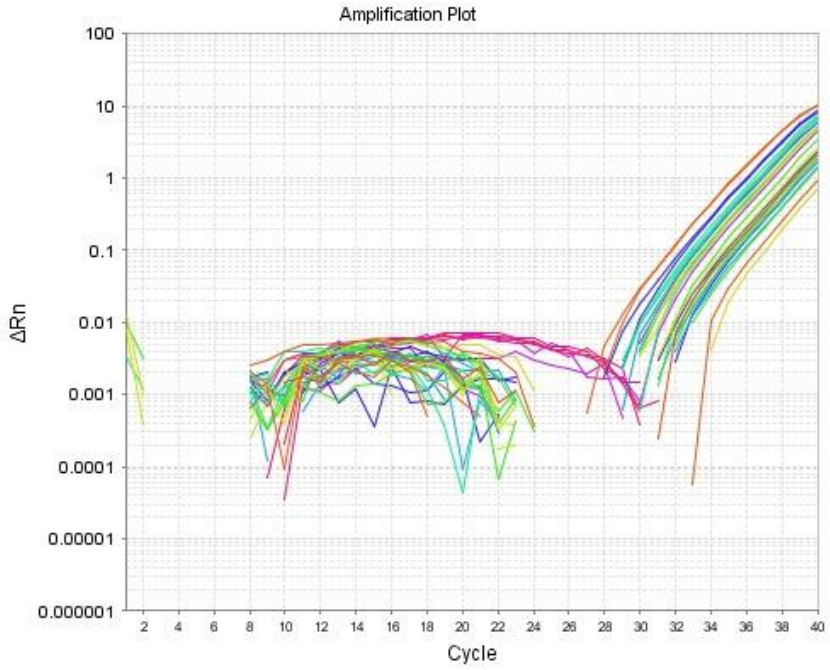

Amplification plot of gene *Bax(1)*.

Annex 2: Melting curves

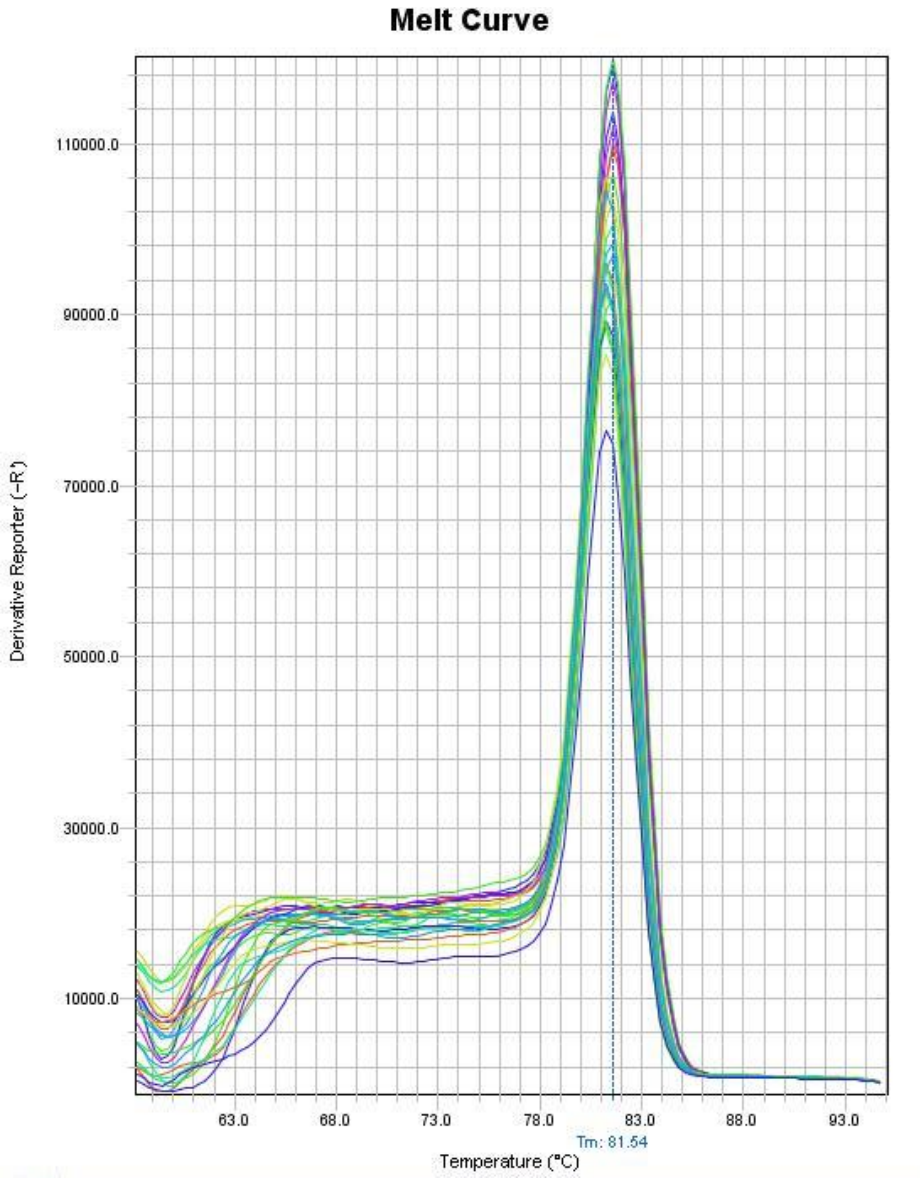

Melting curve of gene *timm23*.

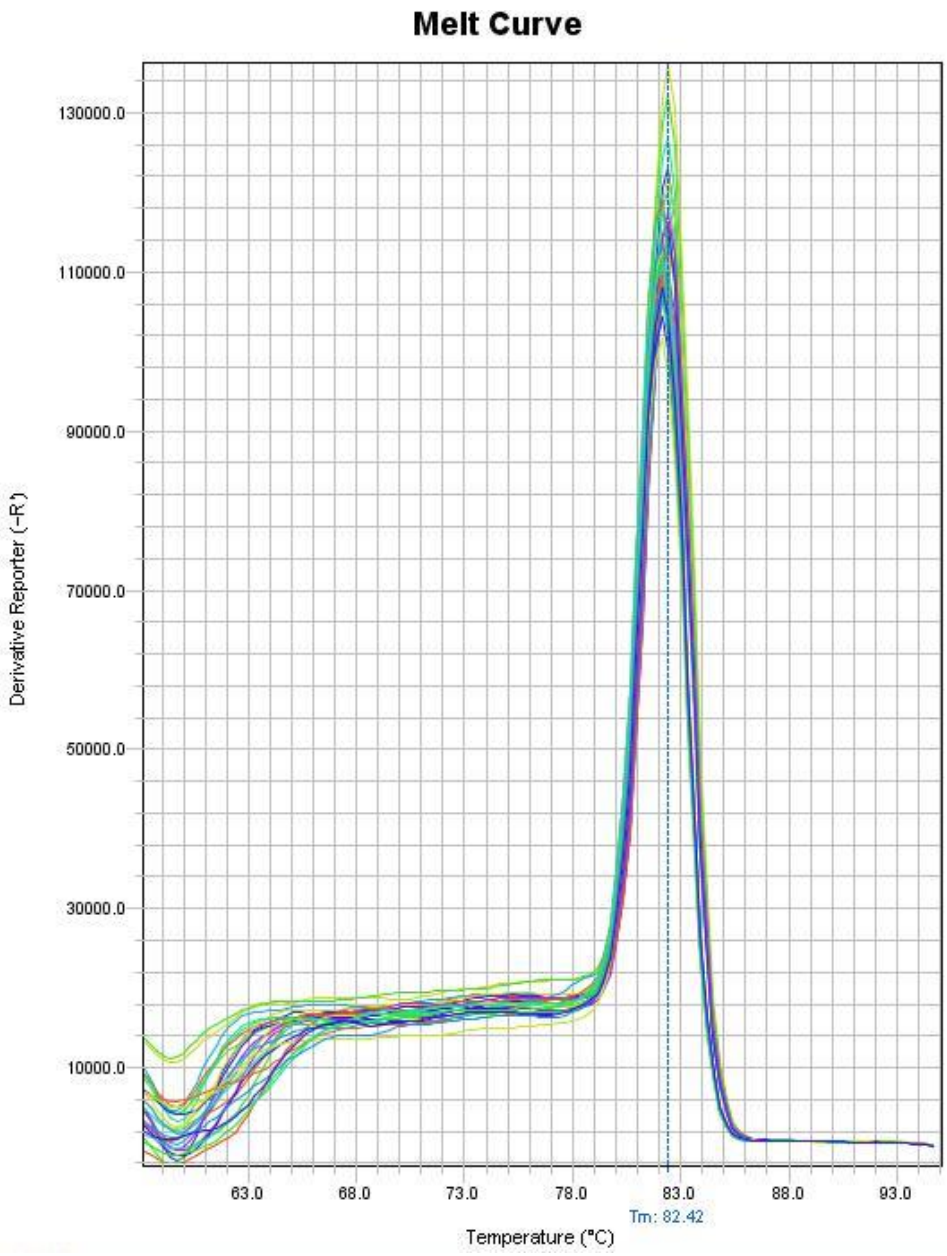

Melting curve of gene *mthsp70*.

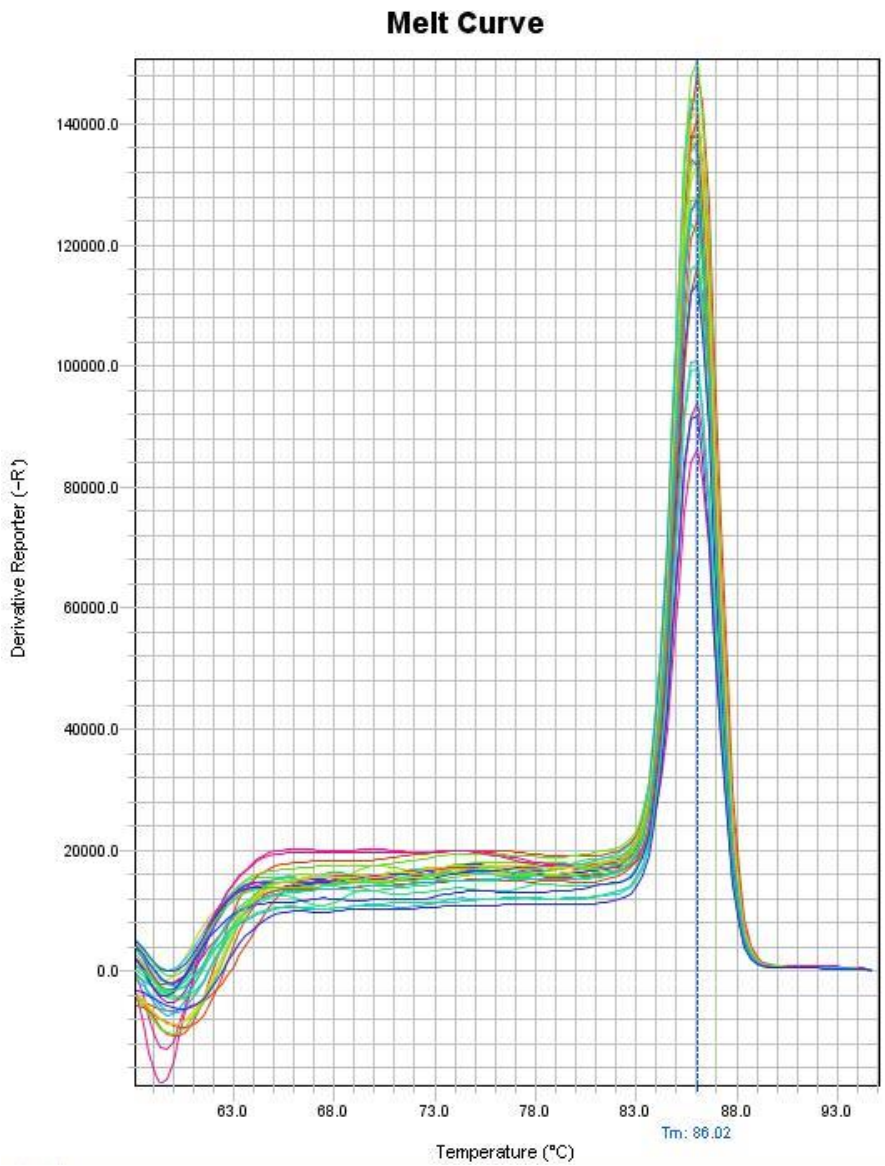

Melting curve of gene *gapdh*.

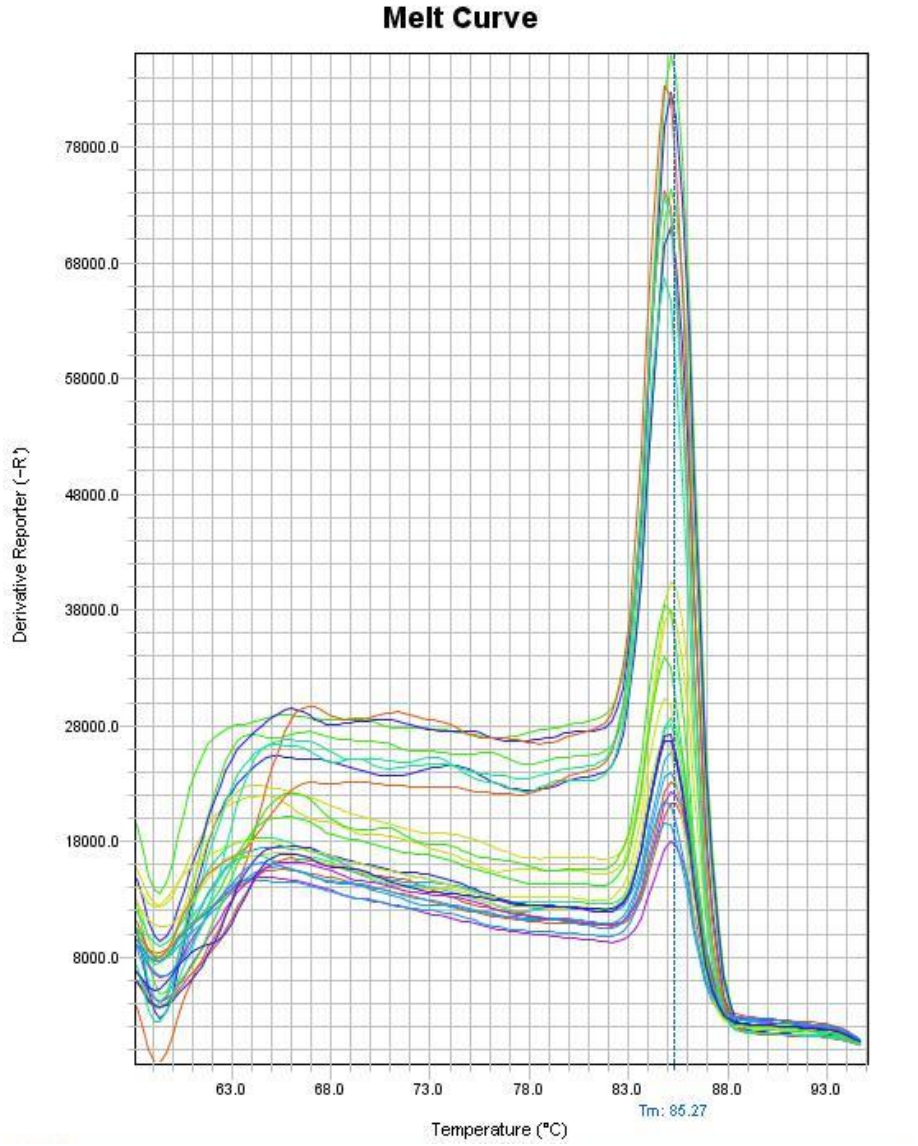

Melting curve of gene *bcl2*.

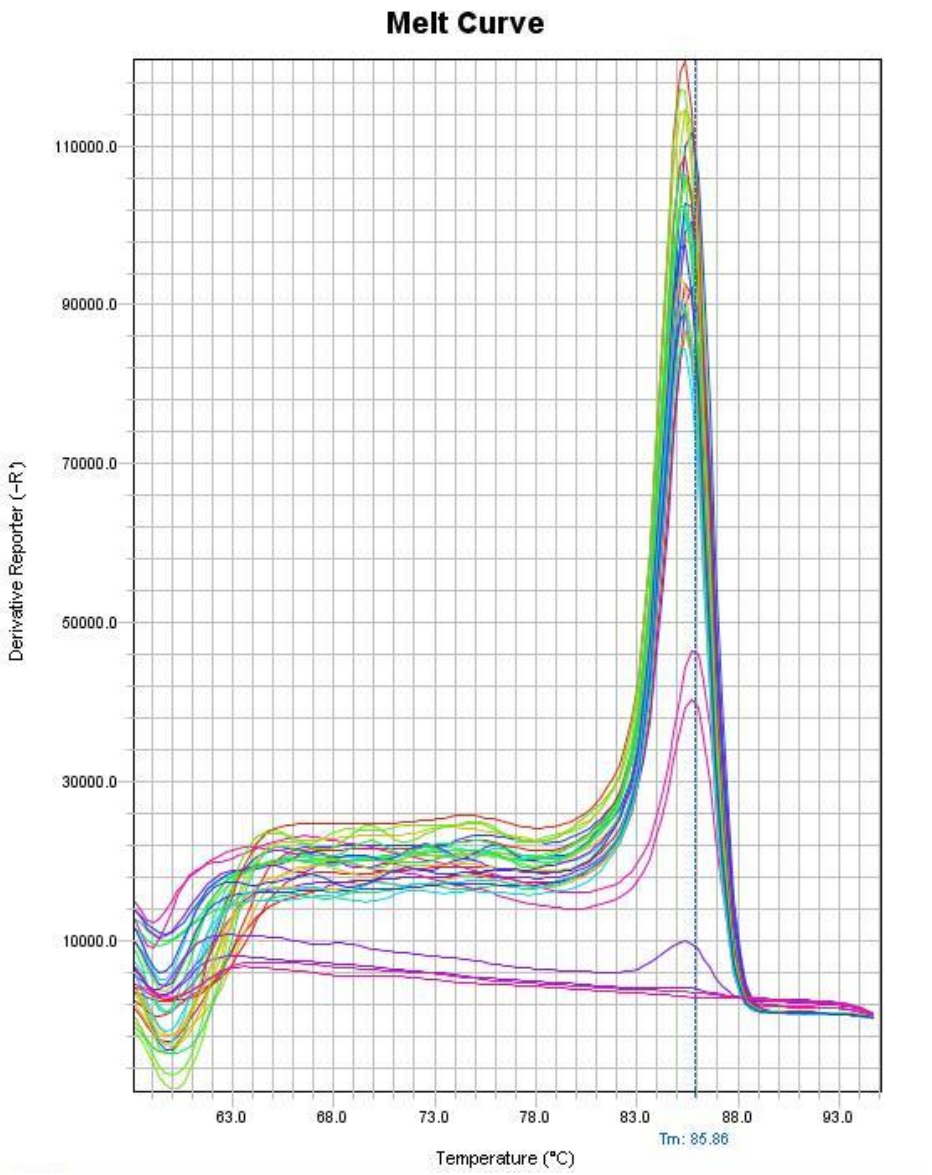

Melting curve of gene *actin*.

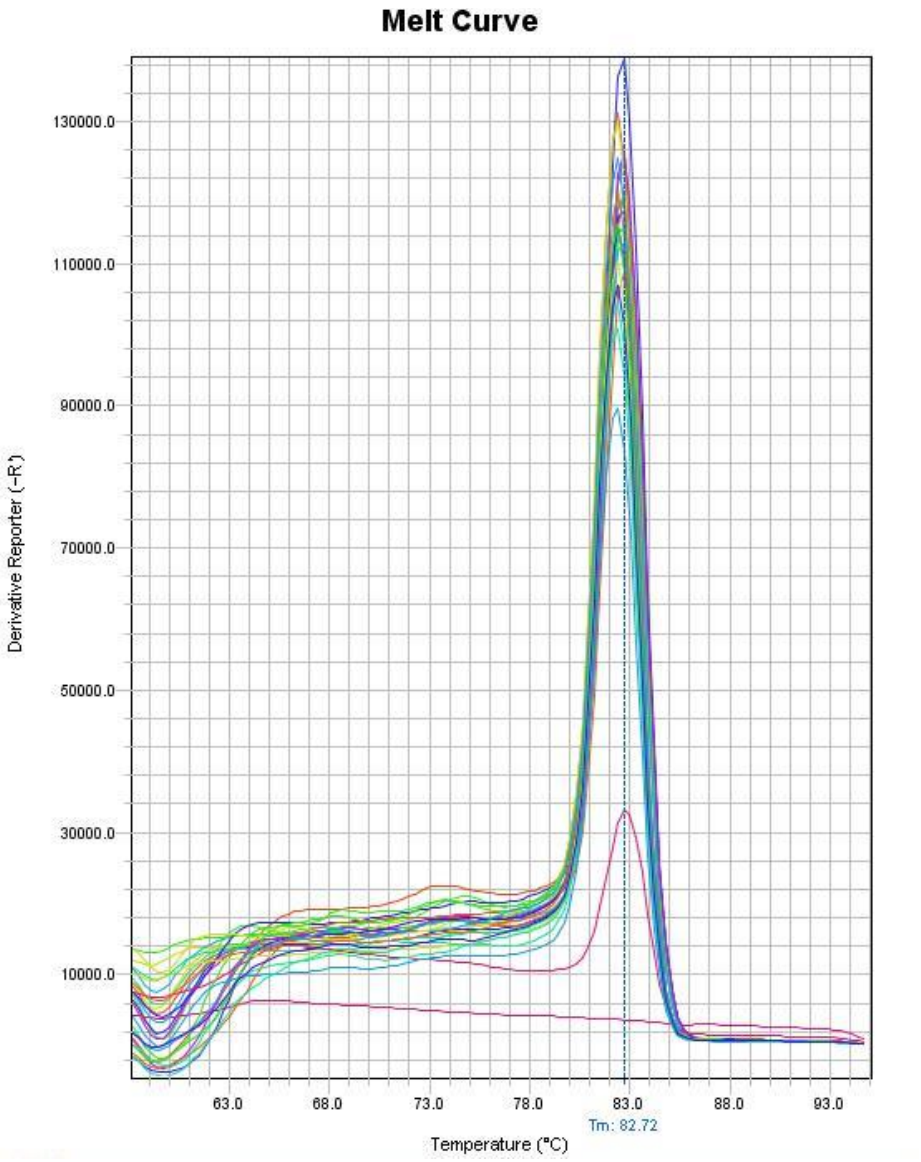

Melting curve of gene *tomm40*.

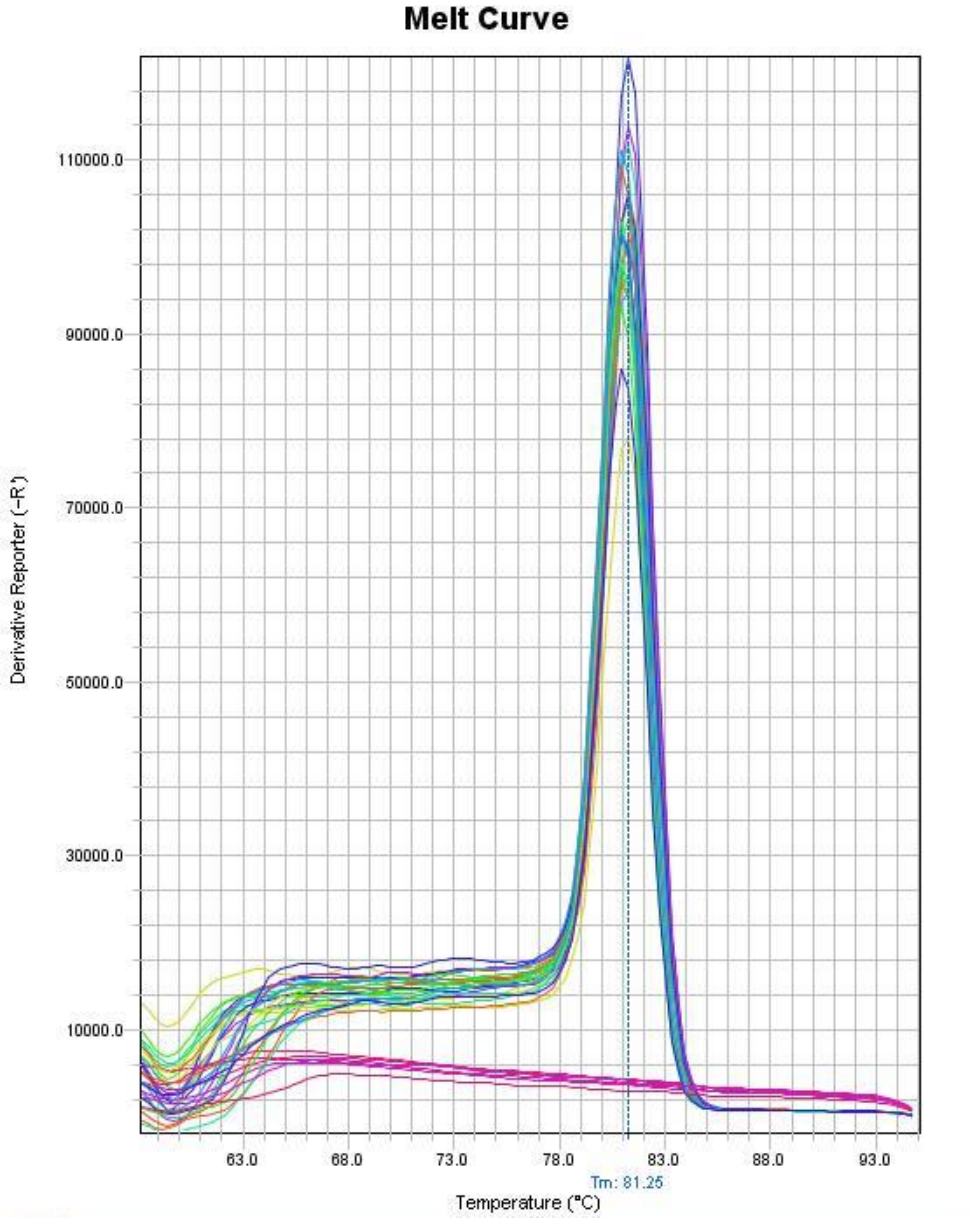

Melting curve of gene *Bax(2)*.

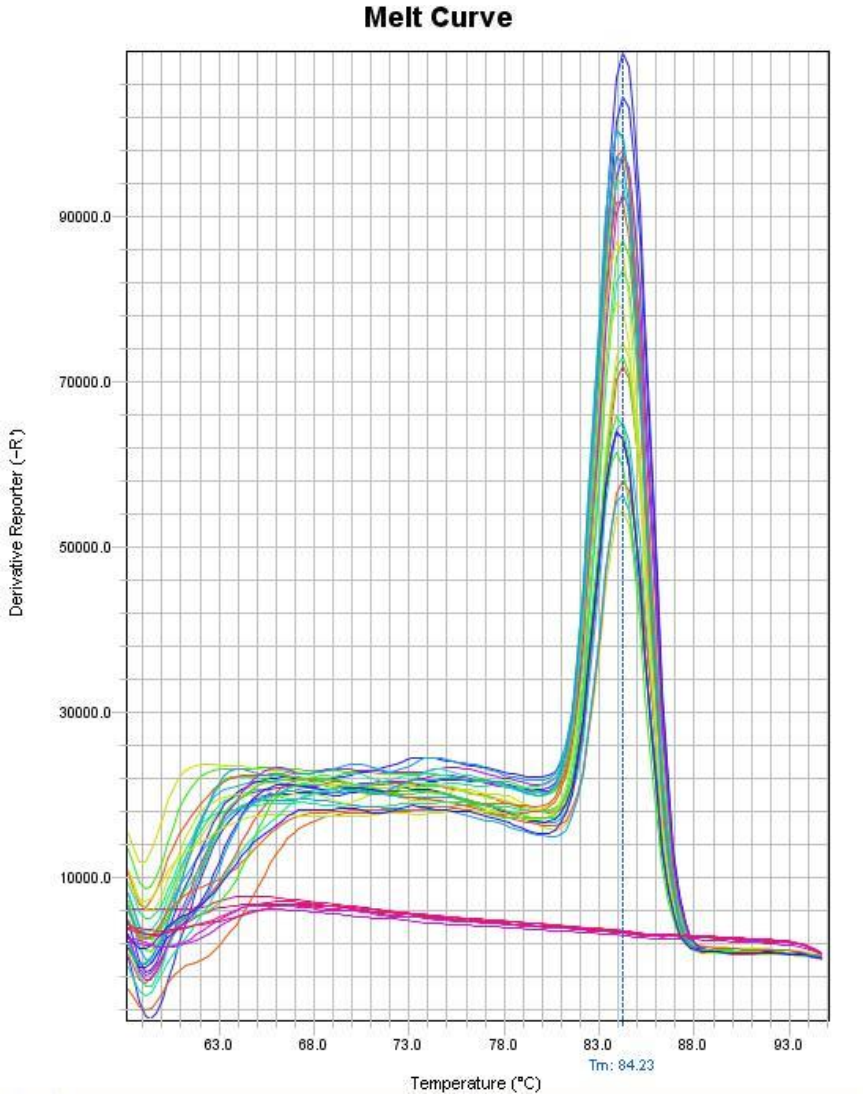

Melting curve of gene *Bax(1)*.

Annex 3: Statistical analysis

TOMM40

Comparaisons multiples :

Variable dépendante: Ct_L

Bonferroni

(I) Time_tomm40	(J) Time_tomm40	Différence moyenne (I-J)	Erreur standard	Signification	Intervalle de confiance à 95 % Borne inférieure	Borne supérieure
eighteen	six	-,7284	,33442	,141	-1,6373	,1805
	twelve	-,4941	,33442	,485	-1,4030	,4148
six	eighteen	,7284	,33442	,141	-,1805	1,6373
	twelve	,2343	,31886	1,000	-,6323	1,1009
twelve	eighteen	,4941	,33442	,485	-,4148	1,4030
	six	-,2343	,31886	1,000	-1,1009	,6323

Calcul basé sur les moyennes observées.

Le terme d'erreur est le carré moyen (Erreur) = ,305.

Comparaisons multiples :

Variable dépendante: Ct_SM

Bonferroni

(I) Time_tomm40	(J) Time_tomm40	Différence moyenne (I-J)	Erreur standard	Signification	Intervalle de confiance à 95 % Borne inférieure	Borne supérieure
eighteen	six	-,2940	,46610	1,000	-1,5895	1,0015
	twelve	,2860	,46610	1,000	-1,0095	1,5815
six	eighteen	,2940	,46610	1,000	-1,0015	1,5895
	twelve	,5800	,38057	,460	-,4778	1,6378
twelve	eighteen	-,2860	,46610	1,000	-1,5815	1,0095
	six	-,5800	,38057	,460	-1,6378	,4778

Calcul basé sur les moyennes observées.

Le terme d'erreur est le carré moyen (Erreur) = ,434.

Comparaisons multiples :

Variable dépendante: Ct_H

Bonferroni

(I) Time_tomm40	(J) Time_tomm40	Différence moyenne (I-J)	Erreur standard	Signification	Intervalle de confiance à 95 % Borne inférieure	Borne supérieure
eighteen	six	,2024	,69504	1,000	-1,6866	2,0914
	twelve	-,0523	,69504	1,000	-1,9412	1,8367
six	eighteen	-,2024	,69504	1,000	-2,0914	1,6866
	twelve	-,2547	,66270	1,000	-2,0557	1,5464
twelve	eighteen	,0523	,69504	1,000	-1,8367	1,9412
	six	,2547	,66270	1,000	-1,5464	2,0557

Calcul basé sur les moyennes observées.

Le terme d'erreur est le carré moyen (Erreur) = 1,317.

T-TEST (6 and 12 week time point)

Tissue	p-value
Liver	0.513652709
SM	0.069919145
Heart	0.631641842

MTHSP60

Comparaisons multiples :

Variable dépendante: Ct_L

Bonferroni

(I) Time_MTHSP60	(J) Time_MTHSP60	Différence moyenne (I-J)	Erreur standard	Signification	Intervalle de confiance à 95 % Borne inférieure	Borne supérieure
Eighteen	Six	-,4994	,47061	,920	-1,7784	,7796
	Twelve	-,4145	,47061	1,000	-1,6935	,8645
Six	Eighteen	,4994	,47061	,920	-,7796	1,7784
	Twelve	,0848	,44871	1,000	-1,1347	1,3043
Twelve	Eighteen	,4145	,47061	1,000	-,8645	1,6935
	Six	-,0848	,44871	1,000	-1,3043	1,1347

Calcul basé sur les moyennes observées.

Le terme d'erreur est le carré moyen (Erreur) = ,604.

Comparaisons multiples :

Variable dépendante: Ct_SM

Bonferroni

(I) Time_MTHSP60	(J) Time_MTHSP60	Différence moyenne (I-J)	Erreur standard	Signification	Intervalle de confiance à 95 % Borne inférieure	Borne supérieure
Eighteen	Six	-,7362	,51005	,524	-2,1538	,6815
	Twelve	-,0457	,51005	1,000	-1,4633	1,3720
Six	Eighteen	,7362	,51005	,524	-,6815	2,1538
	Twelve	,6905	,41646	,370	-,4670	1,8480
Twelve	Eighteen	,0457	,51005	1,000	-1,3720	1,4633
	Six	-,6905	,41646	,370	-1,8480	,4670

Calcul basé sur les moyennes observées.

Le terme d'erreur est le carré moyen (Erreur) = ,520.

Comparaisons multiples :

Variable dépendante: Ct_H

Bonferroni

(I) Time_MTHSP60	(J) Time_MTHSP60	Différence moyenne (I-J)	Erreur standard	Signification	Intervalle de confiance à 95 % Borne inférieure	Borne supérieure
Eighteen	Six	-,3308	,44213	1,000	-1,5324	,8708
	Twelve	-,4443	,44213	,996	-1,6459	,7573
Six	Eighteen	,3308	,44213	1,000	-,8708	1,5324
	Twelve	-,1135	,42155	1,000	-1,2592	1,0322
Twelve	Eighteen	,4443	,44213	,996	-,7573	1,6459
	Six	,1135	,42155	1,000	-1,0322	1,2592

Calcul basé sur les moyennes observées.

Le terme d'erreur est le carré moyen (Erreur) = ,533.

T-TEST (6 and 12 week time point)

Tissue	p-value
Liver	0.874034237
SM	0.160742248
Heart	0.813923682

MTHSP70

Comparaisons multiples :

Variable dépendante: Ct_L

Bonferroni

(I) Time_MTHSP70	(J) Time_MTHSP70	Différence moyenne (I-J)	Erreur standard	Signification	Intervalle de confiance à 95 % Borne inférieure	Borne supérieure
Eighteen	Six	-,2354	,45372	1,000	-1,4685	,9977
	Twelve	-,8974	,45372	,204	-2,1305	,3357
Six	Eighteen	,2354	,45372	1,000	-,9977	1,4685
	Twelve	-,6620	,43261	,445	-1,8377	,5137
Twelve	Eighteen	,8974	,45372	,204	-,3357	2,1305
	Six	,6620	,43261	,445	-,5137	1,8377

Calcul basé sur les moyennes observées.

Le terme d'erreur est le carré moyen (Erreur) = ,561.

Comparaisons multiples :

Variable dépendante: Ct_SM

Bonferroni

(I) Time_MTHSP70	(J) Time_MTHSP70	Différence moyenne (I-J)	Erreur standard	Signification	Intervalle de confiance à 95 % Borne inférieure	Borne supérieure
Eighteen	Six	-,2755	,42479	1,000	-1,4734	,9224
	Twelve	,2045	,42479	1,000	-,9934	1,4024
Six	Eighteen	,2755	,42479	1,000	-,9224	1,4734
	Twelve	,4800	,30037	,415	-,3671	1,3271
Twelve	Eighteen	-,2045	,42479	1,000	-1,4024	,9934
	Six	-,4800	,30037	,415	-1,3271	,3671

Calcul basé sur les moyennes observées.

Le terme d'erreur est le carré moyen (Erreur) = ,271.

Comparaisons multiples :

Variable dépendante: Ct_H

Bonferroni

(I) Time_MTHSP70	(J) Time_MTHSP70	Différence moyenne (I-J)	Erreur standard	Signification	Intervalle de confiance à 95 % Borne inférieure	Borne supérieure
Eighteen	Six	,8135	1,08793	1,000	-2,2104	3,8374
	Twelve	-,4877	1,04686	1,000	-3,3974	2,4220
Six	Eighteen	-,8135	1,08793	1,000	-3,8374	2,2104
	Twelve	-1,3012	,98204	,630	-4,0307	1,4284
Twelve	Eighteen	,4877	1,04686	1,000	-2,4220	3,3974
	Six	1,3012	,98204	,630	-1,4284	4,0307

Calcul basé sur les moyennes observées.

Le terme d'erreur est le carré moyen (Erreur) = 2,630.

T-TEST (6 and 12 week time point)

Tissue	p-value
Liver	0.192883944
SM	0.156982258
Heart	0.20979689

BAX1

In this case, the 18 week time point has been removed and so, only T-tests have been done.

T-TEST (6 and 12 week time point)

Tissue	p-value
Liver	0.671271655
SM	0.15389076
Heart	0.170545603

BCL2

In this case, the 18 week time point has been removed and so, only T-tests have been done.

T-TEST (6 and 12 week time point)

Tissue	p-value
Liver	0.97414662
SM	0.900172733
Heart	0.928062799

BAX2

Comparaisons multiples :

Variable dépendante: Ct_L

Bonferroni

(I) BAX2	(J) BAX2	Différence moyenne (I-J)	Erreur standard	Signification	Intervalle de confiance à 95 % Borne inférieure	Borne supérieure
Eighteen	Six	-,7922*	,13843	,000	-1,1684	-,4160
	Twelve	-,5746*	,13843	,003	-,9508	-,1984
Six	Eighteen	,7922*	,13843	,000	,4160	1,1684
	Twelve	,2177	,13199	,364	-,1410	,5764
Twelve	Eighteen	,5746*	,13843	,003	,1984	,9508
	Six	-,2177	,13199	,364	-,5764	,1410

Calcul basé sur les moyennes observées.

Le terme d'erreur est le carré moyen (Erreur) = ,052.

*. La différence moyenne est significative au niveau ,05.

Comparaisons multiples :

Variable dépendante: Ct_SM

Bonferroni

(I) BAX2	(J) BAX2	Différence moyenne (I-J)	Erreur standard	Signification	Intervalle de confiance à 95 % Borne inférieure	Borne supérieure
Eighteen	Six	-,3784	,26387	,525	-1,1030	,3461
	Twelve	-,0836	,26387	1,000	-,8081	,6410
Six	Eighteen	,3784	,26387	,525	-,3461	1,1030
	Twelve	,2948	,23601	,701	-,3532	,9429
Twelve	Eighteen	,0836	,26387	1,000	-,6410	,8081
	Six	-,2948	,23601	,701	-,9429	,3532

Calcul basé sur les moyennes observées.

Le terme d'erreur est le carré moyen (Erreur) = ,167.

Comparaisons multiples :

Variable dépendante: Ct_H

Bonferroni

(I) BAX2	(J) BAX2	Différence moyenne (I-J)	Erreur standard	Signification	Intervalle de confiance à 95 % Borne inférieure	Borne supérieure
Eighteen	Six	-,1968	,26516	1,000	-,9249	,5313
	Twelve	-,5430	,26516	,184	-1,2711	,1851
Six	Eighteen	,1968	,26516	1,000	-,5313	,9249
	Twelve	-,3462	,23717	,504	-,9974	,3051
Twelve	Eighteen	,5430	,26516	,184	-,1851	1,2711
	Six	,3462	,23717	,504	-,3051	,9974

Calcul basé sur les moyennes observées.

Le terme d'erreur est le carré moyen (Erreur) = ,169.

T-TEST (6 and 12 week time point)

Tissue	p-value
Liver	0.094265002
SM	0.142226896
Heart	0.139870282

TIMM23

Comparaisons multiples :

Variable dépendante: Ct_L

Bonferroni

(I) Time_TIMM23	(J) Time_TIMM23	Différence moyenne (I-J)	Erreur standard	Signification	Intervalle de confiance à 95 % Borne inférieure	Borne supérieure
Eighteen	Six	-,6580	,30339	,143	-1,4825	,1665
	Twelve	-,1203	,30339	1,000	-,9449	,7042
Six	Eighteen	,6580	,30339	,143	-,1665	1,4825
	Twelve	,5377	,28927	,253	-,2485	1,3238
Twelve	Eighteen	,1203	,30339	1,000	-,7042	,9449
	Six	-,5377	,28927	,253	-1,3238	,2485

Calcul basé sur les moyennes observées.

Le terme d'erreur est le carré moyen (Erreur) = ,251.

Comparaisons multiples :

Variable dépendante: Ct_SM

Bonferroni

(I) Time_TIMM23	(J) Time_TIMM23	Différence moyenne (I-J)	Erreur standard	Signification	Intervalle de confiance à 95 % Borne inférieure	Borne supérieure
Eighteen	Six	-,1648	,34333	1,000	-1,1191	,7894
	Twelve	,2822	,34333	1,000	-,6721	1,2364
Six	Eighteen	,1648	,34333	1,000	-,7894	1,1191
	Twelve	,4470	,28033	,410	-,3322	1,2262
Twelve	Eighteen	-,2822	,34333	1,000	-1,2364	,6721
	Six	-,4470	,28033	,410	-1,2262	,3322

Calcul basé sur les moyennes observées.

Le terme d'erreur est le carré moyen (Erreur) = ,236.

Comparaisons multiples :

Variable dépendante: Ct_H

Bonferroni

(I) Time_TIMM23	(J) Time_TIMM23	Différence moyenne (I-J)	Erreur standard	Signification	Intervalle de confiance à 95 % Borne inférieure	Borne supérieure
Eighteen	Six	,4480	,64472	1,000	-1,3224	2,2184
	Twelve	,9188	,64472	,533	-,8515	2,6892
Six	Eighteen	-,4480	,64472	1,000	-2,2184	1,3224
	Twelve	,4708	,57665	1,000	-1,1126	2,0543
Twelve	Eighteen	-,9188	,64472	,533	-2,6892	,8515
	Six	-,4708	,57665	1,000	-2,0543	1,1126

Calcul basé sur les moyennes observées.

Le terme d'erreur est le carré moyen (Erreur) = ,998.

T-TEST (6 and 12 week time point)

Tissue	p-value
Liver	0.115243648
SM	0.110347792
Heart	0.135911173

Expression of genes involved in mitochondrial import, homeostasis and apoptosis.

Présenté par Pauline De Jaeger

Résumé

Ageing is the fundamental biological process of becoming old. It has been defined as the time-dependent decline of functional cellular capacity and stress resistance and is associated with an increased risk for disease. Mitochondria are important organelles that have been implicated as having a major role in ageing. They are central to the control of metabolism, regulation and energetic pathways in eukaryotic cells. When the homeostasis of mitochondria is imbalanced, pathological conditions can occur such as oxidative stress, which results in a decline in mitochondrial function. Mitochondria has also an important role in apoptosis and so, these damages have a big influence in ageing. The genome of mitochondria encodes for only 13 proteins, however for mitochondria to function optimally, they rely on the import of more than 1000 nuclear-encoded proteins. Thus, the mitochondrial protein import machinery plays a key role in the proper functioning of mitochondria. Proteins involved in apoptosis are among some of those that are imported into mitochondria. Apoptosis is a genetically programmed and regulated type of cell death. With ageing, it has been observed that there is a decrease in the potential of apoptosis and this may lead to an increase of cancer incidence.

In this master thesis, we tested the hypothesis that mitochondrial function declines with age due to a reduction in the gene expression of mitochondrial protein import and apoptosis. To test this hypothesis, we used a new model of ageing, the African turquoise killifish. It has the shortest recorded lifespan of a vertebrate in captivity with a reported maximum lifespan ranging between 16 and 24 weeks. For this purpose, primers where designed for each gene and tissues were collected in the fish facilities of KU Leuven. To measure the gene expression, RNA was extracted, cDNA was synthesized and finally, qPCR was performed. As quality control, to ensure the correct PCR product was amplified, melting curves were analysed and PCR product was resolved on an agarose gel.

Overall, we failed to see any significant difference between the three ages that we selected. This may have been due to the variability of the reference genes, the variability of the plates or the small sample size. Furthermore, the samples coming from old fish (18 weeks) seemed to have a higher variability which could be explained by variable and unknown physiological state that influenced the gene expression.

Année académique 2017-2018